Nano Research

Open Access

Review Article

Metal-organic frameworks and covalent-organic frameworks in thermal transport

Pengfei Xu[1,§], Yang Bao[3,§], Changle Liu[1], Stefan Nastic[4], and Biao Xu[1,2]✉

[1] State Key Laboratory of Flexible Electronics (LoFE) & Institute of Advanced Materials (IAM), School of Materials Science and Engineering, Nanjing University of Posts & Telecommunications, Nanjing 210023, China
[2] School of Chemistry and Chemical Engineering, Nanjing University of Science and Technology, Nanjing 210094, China
[3] College of Electronic and Optical Engineering, Nanjing University of Posts & Telecommunications, Nanjing 210023, China
[4] Distributed Systems Group, TU Wien, Argentinierstraße 8, 1040 Vienna, Austria
§ Pengfei Xu and Yang Bao contributed equally to this work.

Cite this article: *Nano Research*, **2026**, *19*, 94908524. https://doi.org/10.26599/NR.2026.94908524

ABSTRACT: Understanding and modulating the inherently low thermal conductivity of crystalline porous frameworks is critical for their deployment in thermal-sensitive applications like gas storage, catalysis, and thermoelectrics. This comprehensive review systematically examines thermal transport fundamentals and recent progress in regulating thermal conductivity for both metal-organic frameworks (MOFs) and covalent organic frameworks (COFs). We detail primary strategies centered on framework architecture design (optimizing density, connectivity, and topology), pore environment modification (via guest molecule inclusion), interfacial bonding enhancement (strengthening vibrational coupling), and composite integration (embedding conductive additives), all aimed at overcoming intrinsic phonon scattering bottlenecks imposed by high porosity and chemical heterogeneity. Key challenges include reconciling structural porosity with phonon transport efficiency, accurately characterizing complex systems, and minimizing interfacial thermal resistance. Addressing these requires synergistic advances in multiscale computational modeling, high-resolution characterization techniques, and targeted interfacial engineering. The review ultimately establishes essential structure–thermal property relationships, providing a foundational guide for the rational design of next-generation framework materials in thermal energy science and technology.

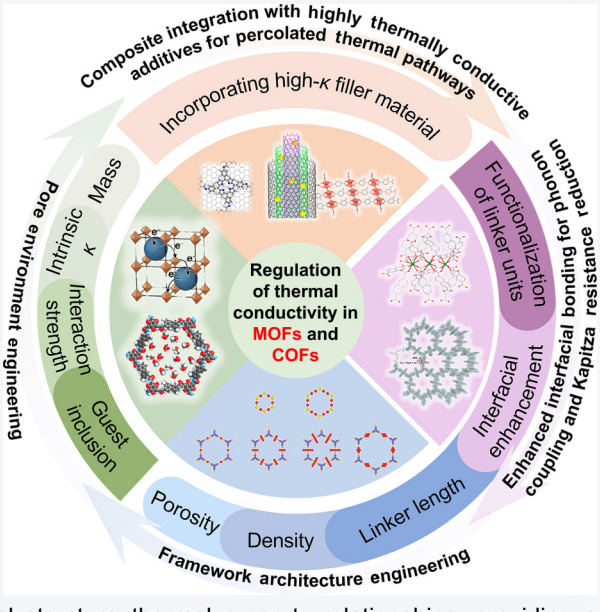

KEYWORDS: metal-organic frameworks (MOFs), covalent organic frameworks (COFs), thermal conductivity, phonon scattering, guest molecules

1 Introduction

Metal-organic frameworks (MOFs) [1, 2] and covalent-organic frameworks (COFs) [3–5] are prominent classes of porous crystalline materials, distinguished by their ordered porosity and significant potential in gas storage [6, 7], separation [8, 9], and catalysis [10, 11]. MOFs form through the coordination bonding of metal ions/clusters with organic linkers, yielding hybrid structures with exceptional surface areas [12, 13]. In contrast, COFs are assembled solely from light elements (C, H, O, N, B) linked by strong covalent bonds (e.g., boronate esters, imines), granting them remarkable rigidity, stability, and predefined geometries [14]. This fundamental distinction in bonding, dynamic coordination bonds in MOFs versus directional covalent bonds in COFs, dictates their overall properties, particularly thermal transport behavior [15, 16]. Specifically, COFs often exhibit superior potential for efficient thermal transport, while MOFs offer versatile catalytic functionality through diverse metal centers but typically exhibit lower intrinsic thermal conductivity (κ). Crucially, phonon-mediated thermal

Received: November 21, 2025; **Revised:** January 13, 2026
Accepted: February 2, 2026

✉Address correspondence to iambxu@njupt.edu.cn

conduction in both material classes is critically modulated by their inherent structural characteristics, including porosity [2, 17, 18], crystallinity [19], bonding strength [20–22], anisotropy [23, 24], defects [3, 21, 25, 26], and phonon scattering mechanisms [18, 25, 27–29]. The exceptional tunability in porosity and structure, lightweight properties, and potential for achieving high thermal conductivity through tailored design enable MOFs/COFs to outperform conventional materials such as metals or polymers in portable electronics, microelectronics cooling and energy-efficient insulation.

Recent progress has thrust MOFs and COFs into thermal science research. The characteristically low intrinsic thermal conductivity of most MOFs makes them attractive for thermal insulation [30, 31]. Their ability to dynamically modulate interfacial thermal conductance upon guest molecule [32, 33] adsorption further opens pathways for adaptive thermal management. Conversely, the rigid, covalently bonded skeletons of COFs, especially two-dimensional (2D) variants, suggest significant potential for high in-plane thermal conductivity [34], positioning them as promising lightweight additives s for advanced thermally conductive composites. Leveraging their tunability, research is rapidly expanding the role of both MOFs and COFs in thermal management solutions across critical sectors like energy conversion [3, 35, 36], microelectronics [37–39], and environmental technologies [31, 40, 41].

Despite extensive investigation into MOFs and COFs for various applications, dedicated research on their thermal transport properties remains nascent, hindering their optimization for thermal management. Coordination-bonded MOF-5 single crystals, with inherent flexibility, typically show values below 1.0 $W \cdot m^{-1} \cdot K^{-1}$ [42, 43]. Covalently bonded COFs offer greater rigidity and anisotropic potential [15]; the experimental κ of COF-300 (pore size < 1 nm) and COF-5 thin films are greater than 1 $W \cdot m^{-1} \cdot K^{-1}$ [23, 44]. Thermal conductivity proves highly sensitive to factors including pore size [18], guest adsorption [11, 29, 45], linker structure [25, 26, 46], and interpenetration [27, 47]. Adsorbed guests, for instance, may suppress conductivity via phonon scattering or enhance it by providing thermal pathways [17, 29, 48, 49]. However, achieving effective thermal control faces substantial bottlenecks: experimental challenges in accurately measuring intrinsic conductivity, especially for powders or films [28, 50, 51]; complexities in theoretical modeling due to force field accuracy and computational demands for large unit cell phonon simulations [45, 52]; difficulties in minimizing interfacial thermal resistance within composites [16, 28]; and the inherent trade-off between optimizing thermal properties and maintaining high porosity. These unresolved issues necessitate focused research.

Addressing these bottlenecks demands breakthroughs across multiple domains: developing reliable high-throughput screening [52–54], constructing precise multi-scale computational models [52, 55], achieving atomic-level control over microstructure and interfaces, and innovating novel *in-situ* measurement techniques [56]. This review critically examines fundamental transport mechanisms, analyzes key influencing factors, explores strategies for achieving high, low, or tunable conductivity, and identifies persistent challenges and emerging solutions. Unlike prior reviews, this comprehensive work uniquely integrates MOFs and COFs, conducting a deeper analysis of their distinct structural characteristics. It specifically highlights how their differing bonding nature (coordinate vs. covalent) and inherent features (e.g., porosity, anisotropy, interlayer interactions) critically govern intrinsic phonon scattering mechanisms and profoundly impact interfacial thermal transport pathways. By integrating experimental and theoretical insights, this review aims to establish a foundation for the rational design and application of MOF/COF materials engineered to meet the escalating demands of advanced thermal management systems, thereby bridging a significant knowledge gap and accelerating innovation in this vital field.

2 Regulation of thermal conductivity

Thermal conduction in both MOFs [16] and COFs [15] is fundamentally governed by phononics, where heat transfer occurs via quantized lattice vibrations (phonons). This process is severely impeded by inherent structural characteristics shared by both material classes: High porosity introduces vast void spaces acting as phonon scattering boundaries, drastically reducing phonon mean free paths [57, 58]; pronounced chemical heterogeneity creates mass mismatch and bond stiffness variations [59] (metal-oxygen clusters vs. organic linkers in MOFs); and anharmonic lattice dynamics [60], exacerbated by framework flexibility and weak inter-unit interactions (e.g., van der Waals forces between layers in COFs [36], organic–inorganic interfaces in MOFs [42]). Consequently, both initial MOFs and COFs theoretically exhibit ultralow thermal conductivities (κ), predominantly below 1 $W \cdot m^{-1} \cdot K^{-1}$ at room temperature [27, 59], as shown in Table 1. This intrinsic property presents significant challenges for applications requiring efficient heat dissipation [42, 49]. Adsorbed gas storage suffers from thermal gradients during rapid adsorption/desorption cycles. Catalysis faces temperature control issues during exothermic reactions. Conversely, their low κ is advantageous for thermal insulation [40, 61] and thermoelectrics, which require ultra-low κ

Table 1 Thermal conductivity (κ) of the MOF/COF-based systems

	Material category	Thermal conductivity (κ) ($W \cdot m^{-1} \cdot K^{-1}$)	Source	References
MOFs	ZIF-8	0.165	Calculated	[62]
	MOF aluminium fumarate	0.07	Calculated	[63]
	NCM@PANI/NF	0.126	Experimental	[64]
	UiO-66	0.11	Calculated	[65]
	UiO-67	0.19		
	Cu-BTC	0.39		
	$Ni_3(HITP)_2$	0.21	Experimental	[58]
	MOF-5	0.3	Experimental	[66]
	HKUST-1	2.2 ± 0.1	Experimental	[49]
	MOF-5	0.32	Experimental	[42]

(Continued)

	Material category	Thermal conductivity (κ) ($W \cdot m^{-1} \cdot K^{-1}$)	Source	References
MOFs	$Ni_3(HITP)_2$	0.32	Experimental	[67]
	$Ni_3(HITP)_2$/CNT30	0.85		
	$Ni_3(HITP)_2$/PEI-CNT30	0.69		
	Cu-BTC/PEDOT:PSS	0.04	Experimental	[68]
	MIL-68(Al)/CN	0.18–7.5	Experimental	[69]
	MIL-53(Al)/CNT	1.3–10.6		
	CNT/ZrBTB-BA(DCB)	2.8–15.3	Experimental	[70]
	CNT/ZrBTB-BA(NMP)	2.2–15.2		
	ZIF-8	0.326 ± 0.002	Experimental	[71]
	ZIF-8(H)	0.1652	Calculated	[72]
	ZIF-8(Br)	0.1418		
	ZIF-8(Cl)	0.1384		
	ZIF-8(CH_3)	0.1743		
	MOF/EG/MWCNT/PW	1.9–2.23	Experimental	[73]
	F_{30}-TAPB-TPA-COF	0.48	Experimental	[74]
	COF-300	0.63 ± 0.08 (cross-plane) 0.32 ± 0.04 (in-plane)	Calculated	[23]
	COF-300-1	27.6 ± 4.8 (cross-plane) 15.1 ± 1.6 (in-plane)		
	TP-COF	0.89 ± 0.14 (cross-plane)	Experimental	[44]
	ICOF-10n-Li/Na	4.04 ± 0.2 (x-direction)	Calculated	[75]
	ICOF-10n-Li/Na	0.74 ± 0.02 (z-direction)	Calculated	
	v2DPA	1.16 ± 0.05	Experimental	[76]
		1.11 ± 0.07	Calculated	
		1.16 ± 0.14	Calculated (EMD)	
		0.34 ± 0.03	Calculated (NEMD)	
	PEG/NF40/T2	0.4823	Experimental	[77]
	PEG/NF70/T2	0.3937		
COFs	COF-5	0.5–5	Calculated	[78]
	COF-102	0.324	Calculated	[51]
	COF-103	0.21		
	COF-105	0.068		
	COF-108	0.015		
	COF-1	1.725 (in-plane) 0.035 (cross-plane)	Calculated	[34]
	C60@COF-1	19.258 (in-plane) 30.155 (cross-plane)		
	COF-6	0.6	Experimental	[79]
	BBO-COF 1	0.391		
	BBO-COF 2	0.677		
	BBO-COF 3	0.581		
	p3HT@BBO-COF 1	0.378		
	p3HT@BBO-COF 2	0.353		
	p3HT@BBO-COF 3	0.402		

alongside high electrical conductivity for competitive figures of merit (ZT) [41].

Actively modulating thermal conductivity is thus essential for unlocking their technological potential [15]. Primary strategies leverage the structure-property relationship (Fig. 1): framework architecture engineering manipulates density [16, 23, 80], linker/node chemistry [22, 46, 81, 82], and topology [25, 53, 83, 84] to optimize phonon pathways; pore environment engineering dynamically alters thermal transport via guest species [29, 32, 34, 45, 58]; interfacial bonding enhancement strengthens vibrational

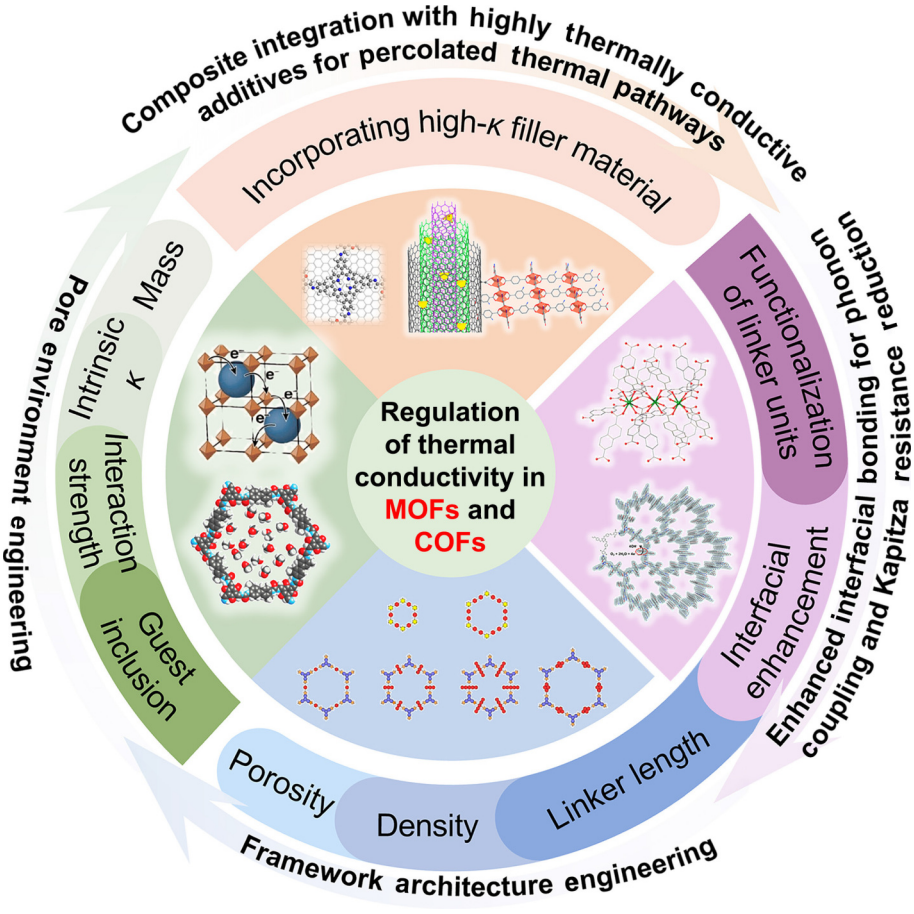

Figure 1 Schematic diagram of the regulation strategies for the thermal conductivity of MOFs and COFs. COF monolayer on graphene. Reproduced with permission from Ref. [87], © American Chemical Society 2022. The structure of MWCNTs-CuBDC-NH_2. Reproduced with permission from Ref. [88], © Elsevier B.V. 2023. The inorganic framework nodes and guest molecules. Reproduced with permission from Ref. [89], © American Chemical Society 2020. Schematic of the pores of methanol-immersed COF-118. Reproduced with permission from Ref. [90], © American Chemical Society 2018. Chained thorium atoms along the [101] direction in $Th(NDC)_2$ MOF (hydrogens omitted for clarity). Th: green; O: red; C: gray. Reproduced with permission from Ref. [91], © American Chemical Society 2018. Structure of the side-chain-modified COF. Reproduced with permission from Ref. [92], © Li, Z. P. et al. 2025. Pore size regulation of COFs. Reproduced with permission from Ref. [15], © American Chemical Society 2023.

coupling within COF layers [24, 34] or at MOF interfaces [22, 45, 52, 85]; and composite integration embeds frameworks within conductive matrices to create percolation networks [34, 35, 86]. Each strategy exploits distinct material characteristics while sharing the overarching goal of overcoming intrinsic phonon scattering bottlenecks.

2.1 Framework architecture engineering

This strategy exploits the inherent synthetic tunability of MOFs [16] and COFs [78] to deliberately design the framework's atomic structure, porosity, and topology to influence phonon generation, propagation, and scattering. The core principle hinges on the direct relationship between atomic connectivity [93], mass mismatch [59], density [24, 80, 94], and phonon mean free paths [34, 51].

The atomic-level structural modulation of MOFs/COFs involves two aspects: unavoidable defective structures formed during synthesis and structural properties responsive to external stimuli. Symmetry-breaking mechanisms, such as engineered defects (e.g., missing-linker defects), exacerbate scattering, reducing phonon mean free paths. Single-atom anchoring creates a localized atomic mass mutation, acting as an excellent coherent phonon scattering center [95]. This significantly degrades thermal transport, as these features are inevitable during practical synthesis [96]. External stimuli such as electric fields [97], magnetic fields [98], or light fields [99] reversibly modulate thermal conductivity by dynamically adjusting the atomic-level framework structures of MOFs/COFs (e.g., bonding alterations, defect density, or lattice distortions), thereby influencing phonon propagation paths and scattering mechanisms to achieve intelligent thermal management responsive to external triggers.

Reducing porosity and increasing framework density generally enhances κ by providing more continuous vibrational pathways [47]. Lengthening organic linkers in MOFs expands pores but reduces density and introduces more low-frequency, easily scattered vibrational modes [29, 59]. Similarly, in COFs, expanding linkers without compensatory densification typically lower κ [54, 81].

Topology plays a critical role: interpenetration creates complex scattering interfaces that generally reduce κ in both MOFs and COFs (e.g., interpenetrated COF-300). Ma et al.'s work [47] on COF-300 interpenetration isomers highlights topology's role (Fig. 2): the denser 7-fold interpenetrated structure (smaller unit cell, 20.4 Å) likely suppresses κ more than the 5-fold variant (28.3 Å) due to increased scattering interfaces.

Specific pore shapes [18, 24, 33, 42] and layer stacking

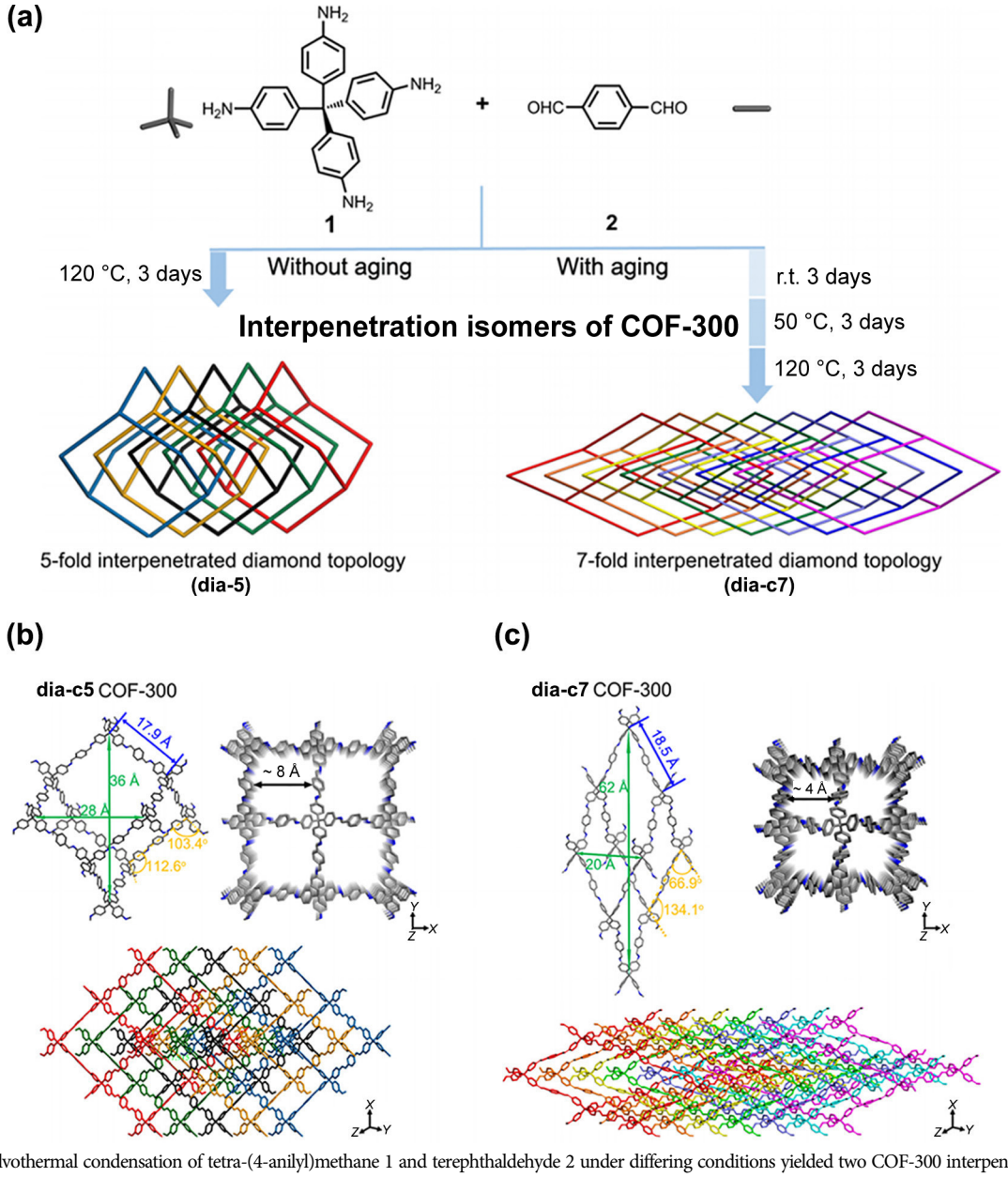

Figure 2 (a) Solvothermal condensation of tetra-(4-anilyl)methane 1 and terephthaldehyde 2 under differing conditions yielded two COF-300 interpenetration isomers. (b) Structural comparison of the dia-c5 (5-fold interpenetrated diamond topology) and dia-c7 variants, featuring a single adamantane-like cage, partial framework along the c-axis, and interpenetrated cages. C: gray, N: blue; H omitted for clarity. Reproduced with permission from Ref. [47], © American Chemical Society 2018.

geometries [100] can either impede or facilitate directional phonon flow. For example, Babaei et al. [18] investigated thermal conductivity regulation in MOFs by designing idealized structures with varied pore shapes (cubic, triangular, and hexagonal channels, inspired by IRMOF-1, FeBDP, and MOF-74, as shown in Figs. 3(a) and 3(b)) and pore sizes (1.0–2.7 nm, controlled by adjusting atoms per unit cell from 7 to 22). Employing molecular dynamics with quartic-bond and harmonic-angle potentials calibrated to achieve typical MOF conductivity (~ 1 $W \cdot m^{-1} \cdot K^{-1}$), they found that thermal conductivity decreases with increasing pore size due to reduced bonded interaction density, scaling inversely with pore cross-sectional area. Additionally, hexagonal-channel MOFs exhibited the highest conductivity parallel to channels (Fig. 3(c)), while perpendicular-direction conductivity decreased as 1/pore size and parallel-direction as 1/pore size^2 for channel geometries (Figs. 3(d) and 3(e)).

The feasibility of this method is exceptionally high due to the vast libraries of building blocks and advanced computational tools. Molecular dynamics simulations (e.g., Green-Kubo formalism [101, 102] using specialized potentials like MACE-MP-MOF0 for MOFs [52] or classical force-fields for COFs [51, 60]) enable predictive design by establishing structure-thermal conductivity relationships before synthesis, guiding the selection of linkers, nodes, and topologies for targeted κ. Computational studies on MOFs like the IRMOF series quantitatively demonstrate architecture's impact [59]: elongating linkers (MOF-5 → IRMOF-10 → IRMOF-16) reduces density and plunges κ from 0.29 to 0.07 $W \cdot m^{-1} \cdot K^{-1}$. Conversely, dense frameworks like UiO-66 (Zr-based nodes, $\kappa \sim 0.87$ $W \cdot m^{-1} \cdot K^{-1}$) and MOF-505 (interconnected Cu-paddlewheels, $\kappa \sim 1.2$ $W \cdot m^{-1} \cdot K^{-1}$) achieve higher conductivities. In COFs, structural engineering manifests differently. Giri et al. [78] showed that increasing linker length with densification (COF-1 to

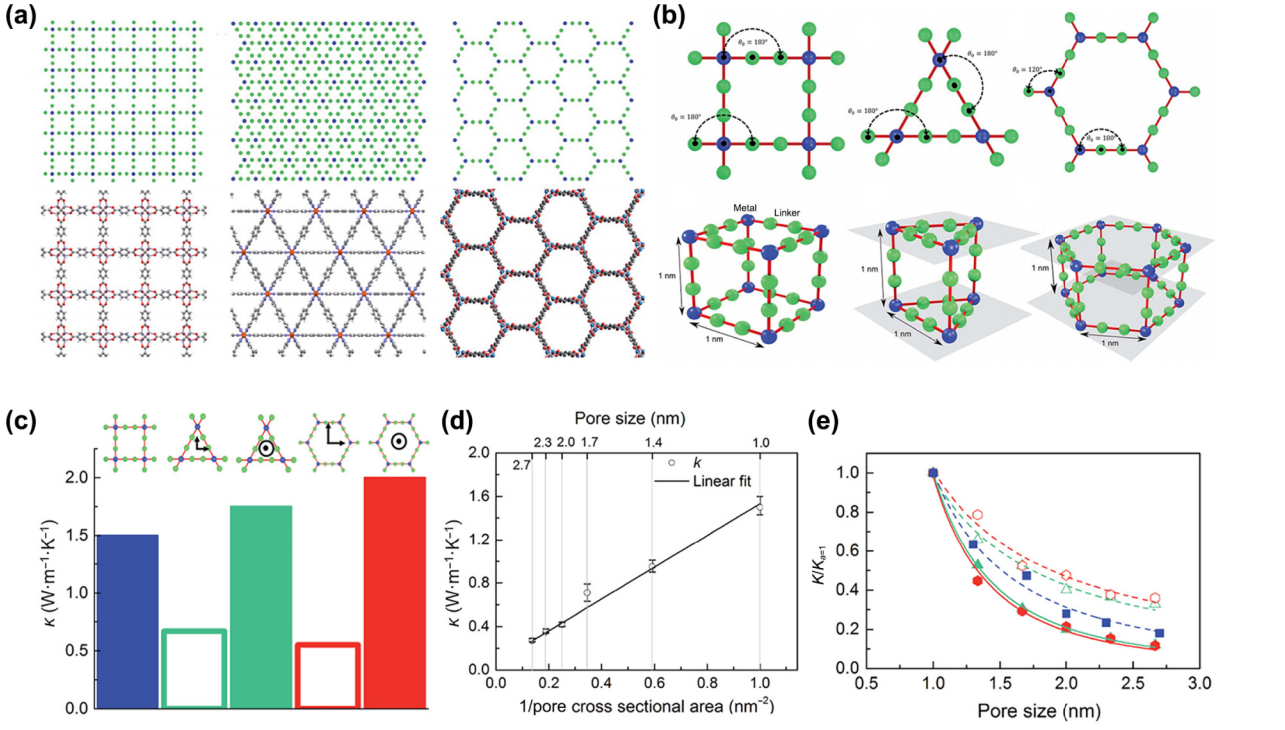

Figure 3 (a) Idealized vs. actual cross-sections: cubic (IRMOF-1), triangular-channel (FeBDP), and hexagonal-channel (MOF-74) structures. (b) Unit cell bonds/angles and lattice plane spacings for cubic, triangular-, and hexagonal-channel systems. (c) Thermal conductivity (κ) of MOFs with varied pore shapes at fixed cross-sectional area (1 nm^2). (d) κ of gas-free cubic structures vs. pore size (top) and 1/pore size^2 (bottom). (e) κ vs. pore size: hexagonal/triangular-channel MOFs parallel (filled) and perpendicular (empty) to channels, with cubic reference (filled squares). Reproduced with permission from Ref. [18], © Royal Society of Chemistry 2017. The lines in (b) represent power law fits to the data points, with exponents of −1.78 (squares), −2.13 (solid hexagons), −2.19 (solid triangles), −1.07 (open hexagons), and −1.14 (open triangles).

COF-1-2R, density: 0.99 to 0.71 g·cm^{-3}) enhanced κ from 2.5 to 5 W·m^{-1}·K^{-1} along the arm-chair direction by reducing boundary scattering. Moscarello et al. [79] found that the use of a planar triazine-core building unit in BBO-COF 3, compared to the planar benzene-core unit in BBO-COF 2, enables stronger interlayer π–π interactions, thereby enhancing phonon coupling and thermal conductivity, as shown in Figs. 4(a)–4(c).

2.2 Pore environment engineering (guest inclusion)

This strategy leverages the dynamic porosity of MOFs/COFs (and potentially large-pore COFs) by introducing guest molecules [32, 44, 45, 90, 103] into the pores to reversibly alter thermal transport. The principle involves two competing, guest-density-dependent effects: enhanced phonon scattering where adsorbed molecules act as additional point defects, scattering lattice phonons and reducing their mean free path and contribution to κ [17, 33]; and guest-phase conduction where the confined guest molecules themselves conduct heat via intermolecular collisions and collisions with the pore walls (gas/solid conduction) [24]. For flexible frameworks like MIL-53 [104–106], adsorption-induced strain ("breathing effect") can drastically modulate κ by altering bond force constants and phonon spectra through micro-expansion/contraction. Moreover, guest molecule regulation, such as through photoisomerization [107–110], enables on-demand thermal conductivity control. Light-induced conformational changes disrupt atomic arrangements, triggering localized lattice strain or defect redistribution that modulates phonon scattering cross-sections and propagation barriers, facilitating photoresponsive thermal management.

The feasibility of this strategy is highest for MOFs due to typically higher pore volumes, adsorption affinities and structural adaptability, also relevant for large-pore COFs. The modulation is inherently reversible and tunable by guest pressure/loading, offering real-time control. The net effect on the total system thermal conductivity ($\kappa = \kappa_{lattice} + \kappa_{guest}$) depends critically on the relative strength of these opposing mechanisms and the guest's intrinsic thermal conductivity. At low-to-moderate loadings, scattering typically dominates, reducing κ. At very high loadings (near saturation or high pressure), κ_{guest} increases significantly and can outweigh the reduced $\kappa_{lattice}$, leading to a net enhancement. The guest type (mass, interaction strength with the framework, intrinsic κ_{guest}) is crucial. Heavier molecules scatter phonons more effectively, while high-κ_{guest} molecules (e.g., H_2) boost κ more. Computational methods (Green-Kubo EMD, NEMD, phonon analysis like spectral energy density) [49] and experimental techniques (Transient Plane Source under pressure) are vital for probing these mechanisms [51].

Semelsberger et al. [111] provided key experimental evidence using MOF-5 compacts: intrinsic $\kappa_{isotropic}$ under vacuum was low (~ 0.13 W·m^{-1}·K^{-1}), but introducing high-pressure gases (H_2, He) dramatically enhanced κ. A rapid increase occurred between 0-10 bar, plateauing above ~ 50–60 bar, yielding over a two-fold enhancement (Fig. 5(a)). Crucially, H_2 induced a larger enhancement than He at equivalent pressures, directly correlating with H_2's higher intrinsic thermal conductivity, proving the dominance of gas-phase conduction at high loadings. Babaei and Wilmer's MD simulations [49] on idealized pores (Figs. 5(b)–5(d)), and Babaei filled with methane elucidated the atomic-scale mechanism for the initial reduction (Figs. 5(e) and 5(f)): adsorbed methane significantly reduced κ as gas density increased. Spectral

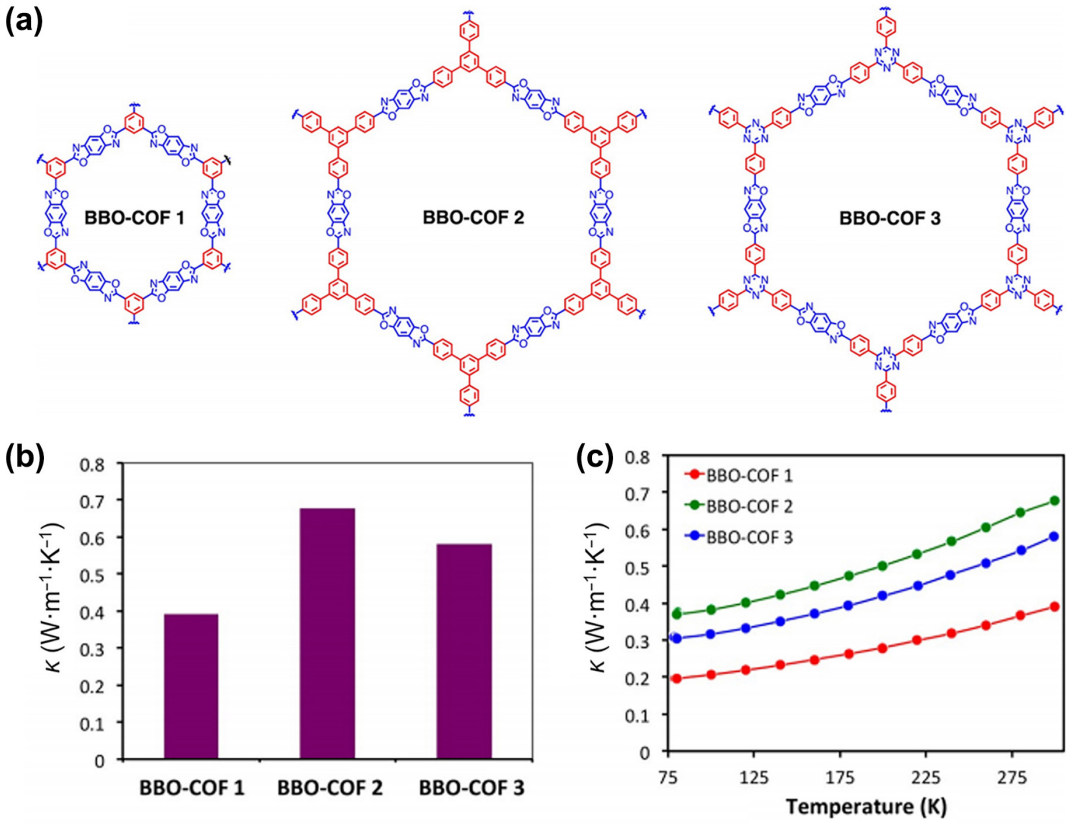

Figure 4 (a) Molecular structures. (b) κ at 300 K. (c) Temperature-dependent κ profiles of BBO-COFs 1–3. Reproduced with permission from Ref. [79], © American Chemical Society 2022.

energy density analysis quantified decreased phonon lifetimes, especially for low-frequency modes, with the scattering rate scaling linearly with gas density. This confirmed phonon scattering by collisions with adsorbed molecules as the primary mechanism for initial κ reduction. While prominent in MOFs, pore environment engineering in COFs is less explored but potentially applicable to frameworks with very large, accessible pores capable of significant guest uptake, impacting vibrational dynamics.

2.3 Enhanced interfacial bonding for phonon coupling and kapitza resistance reduction

This strategy focuses on strengthening the vibrational coupling between structural components, primarily within COF layers or at interfaces in MOF-composites, to reduce interfacial thermal resistance (Kapitza resistance) [28, 93] and enhance phonon transmission.

In COFs, the weak van der Waals forces between stacked 2D layers [15, 79] are a major source of phonon scattering. Introducing strong intermolecular interactions, such as hydrogen bonding networks [36, 112, 113] between layers or side-chain interdigitation (Figs. 6(a)–6(e)) [19, 36, 92], can significantly stiffen the interlayer coupling, leading to longer phonon mean free paths and higher out-of-plane thermal conductivity. While explicit κ measurements on H-bonded variants are still emerging, computational studies strongly support the principle. Incorporating complementary H-bond donors and acceptors on adjacent COF layers can create a percolating network of strong, directional interactions, significantly increasing the force constants associated with interlayer vibrations compared to weak vdW forces. This stiffening suppresses low-frequency, scattering-prone vibrational modes and facilitates higher-frequency phonon transmission across the interface. Chemical modifications like judicious functionalization of linker units can create these bonding bridges. The feasibility relies on targeted covalent functionalization or post-synthetic modification strategies to introduce H-bond donors/acceptors or other interacting groups without compromising crystallinity. Computational modeling helps predict the impact of specific interactions on interfacial force constants [114–117] and phonon spectra [75, 118–120].

For MOFs, while intrinsic interfacial enhancement within the framework is less direct, this concept becomes highly relevant in the context of composite materials [121–124], where minimizing interfacial thermal resistance between the MOF matrix and a high-κ additive is crucial. Moscarello et al. [125] developed MOF composites (e.g., HKUST-1@BNNS-PEI) by mechanochemical assembly (Fig. 7(a)), involving ball milling to exfoliate boron nitride into nanosheets (BNNS) and form amino-B bonds with polyethyleneimine (PEI), followed by anchoring metal ions and growing MOFs to create self-supporting foams via freeze-drying. They measured thermal conductivities using the transient hot-wire method, finding that pure MOFs had low values (≈ 0.075–0.091 $W \cdot m^{-1} \cdot K^{-1}$), while MOFs@BNNS composites showed modest improvements (29.7%–40.0%). However, MOFs@BNNS-PEI exhibited substantial thermal conductivity enhancements (105.5%–128.0%) due to PEI acting as a thermal bridge, which reduced interfacial thermal resistance by forming a continuous conductive network (Fig. 7(b)). In contrast, composites without PEI-bonding had limited gains due to loose connections. Thermal diffusivity tests further confirmed reduced resistance enabled faster heat transfer in the foams, despite larger pores typically lowering

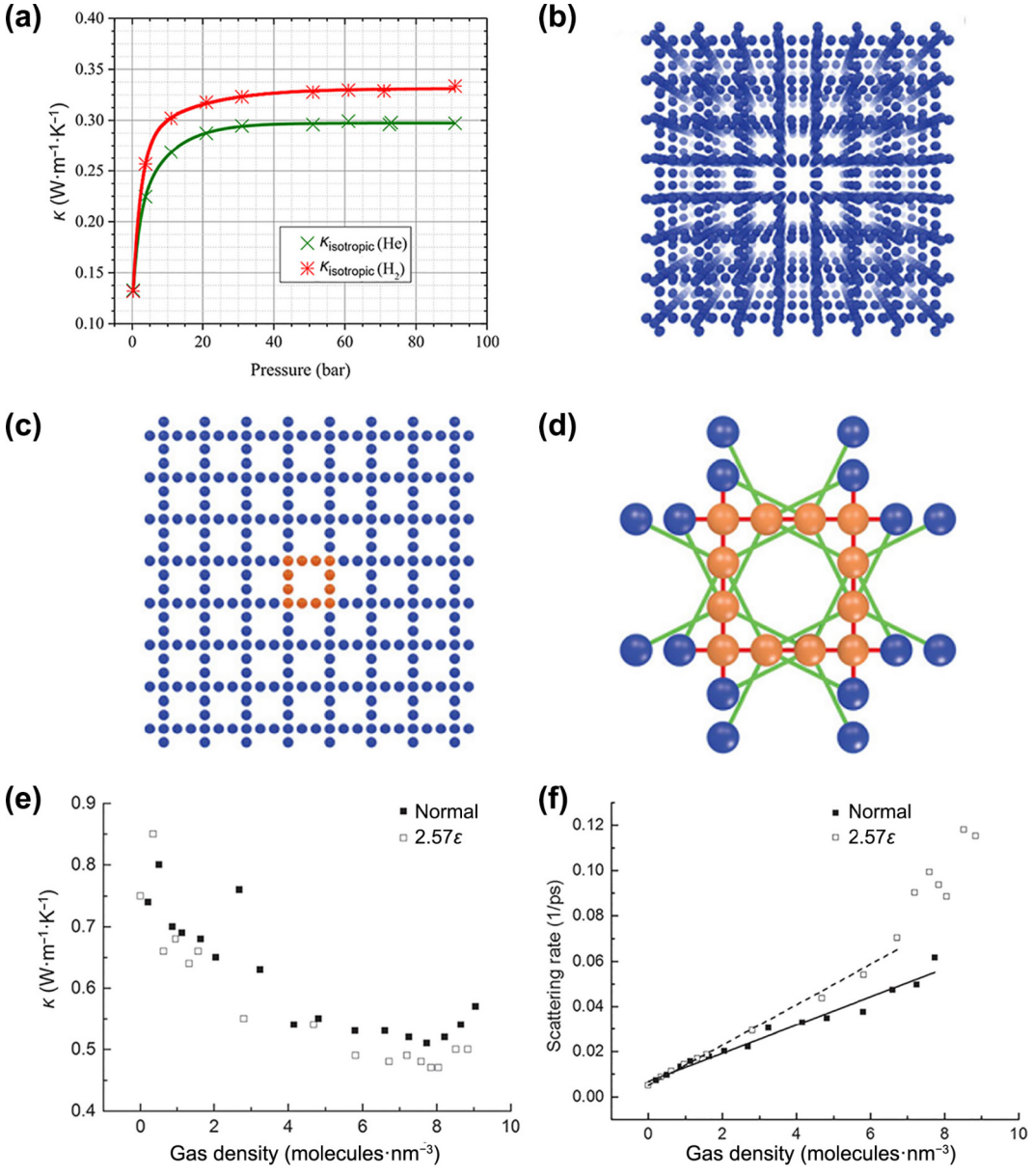

Figure 5 (a) Isotropic κ of neat MOF-5 compacts vs. absolute pressure and gas type at 16 °C. Reproduced with permission from Ref. [111], © Hydrogen Energy Publications, LLC. Published by Elsevier Ltd. 2016. (b) Simulated idealized porous crystal: 8 × 8 × 8 cubic unit cells (7 basis atoms each). (c) Atomic configuration per cube: 8 corners + 24 edges (orange-highlighted cube; 4 corners + 8 edges visible in 2D view). (d) Contrasting bonding environments: corner vs. edge atoms; stronger proximal bonds (red) vs. weaker distal bonds (green). (e) κ vs. loaded gas density. (f) Scattering rate of lowest-frequency mode vs. gas density. Reproduced with permission from Ref. [49], © American Physical Society 2016.

diffusivity (Fig. 7(c)). Strategies analogous to interfacial bonding enhancement, such as covalent functionalization of the MOF surface to improve chemical compatibility with the additive or using coupling agents, are actively researched to strengthen the vibrational coupling and reduce this resistance.

2.4 Composite integration with highly thermally conductive additives for percolated thermal pathways

This strategy directly counteracts the low thermal conductivity of neat MOF or COF powders/pellets by incorporating highly thermally conductive materials (e.g., expanded natural graphite (ENG) [66, 126], carbon nanotubes (CNTs) [88, 127–129], graphene [87, 130–132], metal particles [133, 134]) that form a percolating network throughout the porous matrix. The principle relies on the additives providing low-resistance pathways ("thermal highways") for heat flow, effectively bypassing the highly resistive framework material. Achieving percolation (an interconnected additive network) is critical. The effectiveness of these methods depends on: additive loading (must exceed percolation threshold) [15], additive morphology [58, 135] and dispersion [136, 137] (optimizing connectivity and minimizing voids), intrinsic κ of the additives, and composite compaction density. Researchers must make careful engineering trade-offs. High additive loadings (> 5 wt.%–10 wt.%) can significantly reduce the volumetric adsorption capacity. Achieving good additive dispersion and strong interfacial contact without damaging the delicate framework structure during processing is challenging. Despite this, composite formation offers the most dramatic and practically scalable pathway

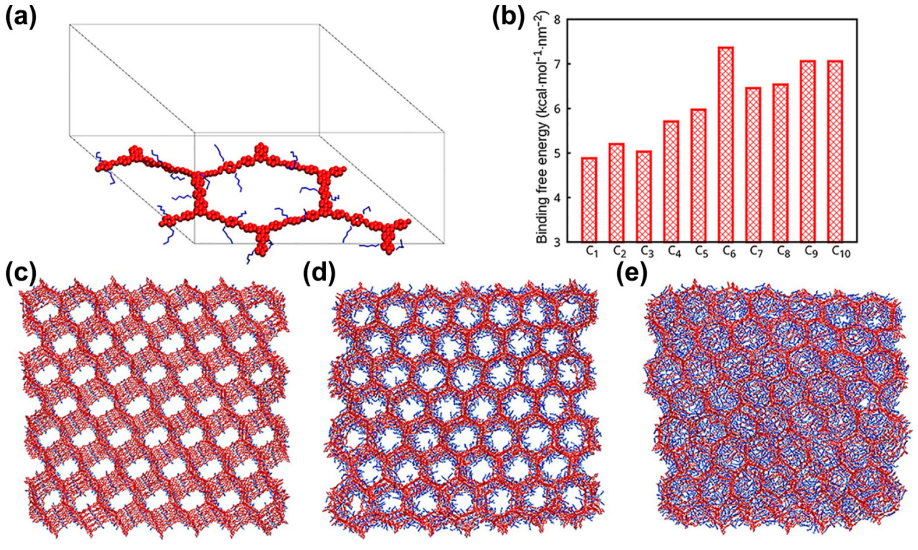

Figure 6 (a) MD-simulated side views of C6 COF monolayer. (b) Calculated layer-stacking binding free energy. (c)–(e) Simulated structures of C2, C6, and C10 COFs. (a) and (b)–(e) Red: COF framework; blue: alkyl chains. Reproduced with permission from Ref. [19], © American Chemical Society 2023.

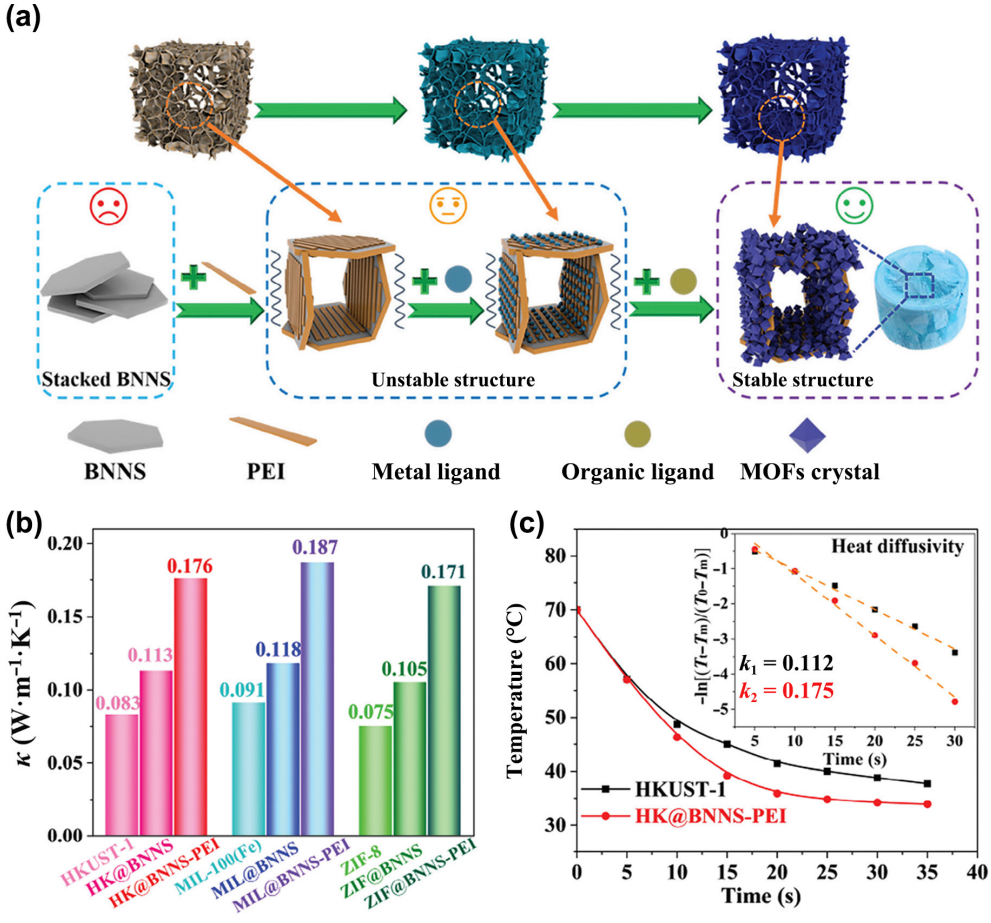

Figure 7 (a) HK@BNNS-PEI fabrication process. (b) κ of MOF powder, MOF@BNNS, and MOF@BNNS-PEI. (c) Temperature evolution of HK@BNNS-PEI vs. HKUST-1 powder; inset: thermal diffusivity coefficient. Reproduced with permission from Ref. [125], © Wiley-VCH GmbH 2024.

to achieve order-of-magnitude κ improvements necessary for device integration, particularly in thermal management for energy storage applications.

Lin et al. [136] synthesized hybrid fillers by growing ZIF-8 MOFs on CNTs, creating CNT@ZIF-8 composites (Fig. 8(a)). These fillers were integrated into mixed-matrix membranes (MMMs) to enhance interfacial compatibility and dispersion, leveraging CNTs' conductivity and ZIF-8's molecular sieving properties. Kang et al. [137] developed metal hydroxide/GO (graphene oxide) membranes via vacuum filtration, where metal hydroxide nanosheets served as metal sources (Fig. 8(b)). MOF fillers were then generated within the layered GO matrix via coordination bonds with organic linkers.

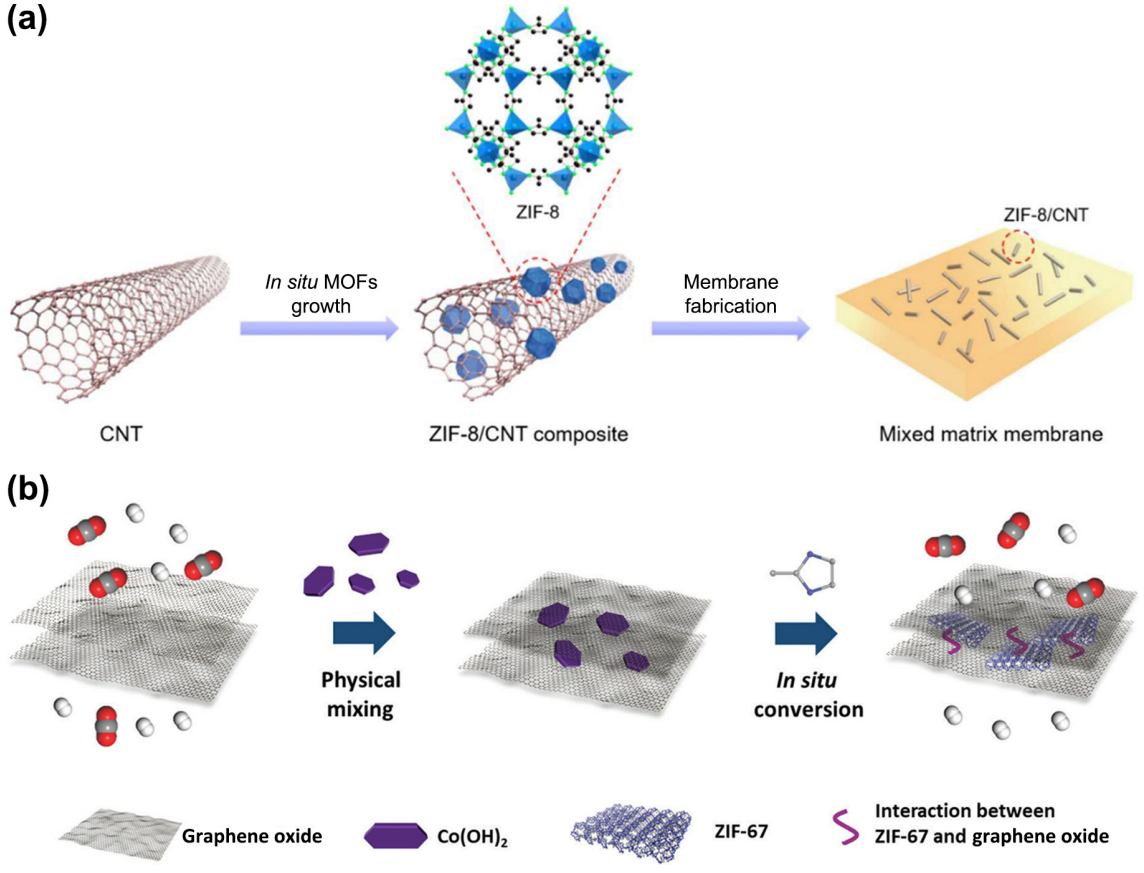

Figure 8 (a) Schematic of 6FDA-durene MMM with ZIF-8-decorated CNTs. Reproduced with permission from Ref. [136], © Royal Society of Chemistry 2016. (b) Gas-separation sandwich membrane via 2D confinement strategy. Reproduced with permission from Ref. [137], © Royal Society of Chemistry 2018.

This strategy exploited GO's 2D confinement to ensure uniform filler distribution and ultrathin membrane thickness while strengthening MOF-GO integration. Purewal, Siegel, and colleagues pioneered this approach for MOF-5 cryo-adsorptive hydrogen storage [66]. Neat MOF-5 pellets had $\kappa < 0.1$ W·m^{-1}·K^{-1}, insufficient for rapid tank refueling heat dissipation. Integrating 10 wt.% ENG into MOF-5 monoliths compacted to 0.5 g·cm^{-3} increased κ by a factor of 5 compared to neat pellets at the same density. This was attributed to a percolating graphite network acting as an efficient heat conduit. Optimization was needed as higher ENG loadings reduced H_2 capacity.

While less prevalent than for MOFs, composite approaches are also viable for COFs. Incorporating high-κ fillers like nickel particles into COF matrices follows the same fundamental principles. Yang et al. [77] addressed the optimization of thermal conductivity in their composite phase change materials (CPCMs) by integrating nickel foam (NF) as a high-thermal-conductivity support structure for the covalent-organic framework (COF TpPa). They prepared NF/TpPa hybrids (Fig. 9(a)) via solvothermal growth of TpPa on NF scaffolds with varying pore sizes (40, 60, and 70 PPI, PPI indicates the pore density of nickel foam, defined as holes per inch, with an inverse relationship to pore size), leveraging NF's intrinsic high thermal conductivity, low cost, and robust mechanical properties to overcome the inherent low thermal conductivity limitations of both pure PEG and COFs. The resulting PEG/NF/TpPa CPCMs exhibited significantly enhanced thermal conductivity compared to pure PEG (1.9 times higher) and PEG/TpPa composites without NF (Fig. 9(b)). Furthermore, they experimentally verified that the thermal conductivity of the CPCMs positively correlated with the pore size of the NF used, confirming NF's critical role in facilitating rapid heat transfer within the composite structure. Infrared thermal imaging validated the improved thermal diffusion performance under heating conditions (Fig. 9(c)).

The key challenges remain preserving COF crystallinity/porosity during composite processing and minimizing interfacial thermal resistance at the COF/additive interface. Research is ongoing to optimize additive selection (e.g., matching surface chemistry), functionalization strategies to improve interfacial bonding [21, 138, 139], and processing techniques (e.g., *in-situ* growth of COFs on additives) [140, 141] to maximize κ enhancement while retaining COF functionality for applications like thermoelectrics or electronics thermal management.

3 Current challenges

The fundamental challenge in regulating the thermal conductivity (κ) of MOFs and COFs stems from multiple dimensions. Key intrinsic material limitations including weak coordination bonds in MOFs, anisotropic covalent networks in COFs, and porosity-induced phonon scattering. Characterization bottlenecks stem from the scarcity of high-quality single crystals and significant Kapitza resistance at grain boundaries and composite interfaces. The challenges in theoretical research are attributed to the limitations in force fields for simulation. Overcoming these intertwined obstacles is crucial for advancing their application in thermal energy management, gas storage, and thermoelectrics.

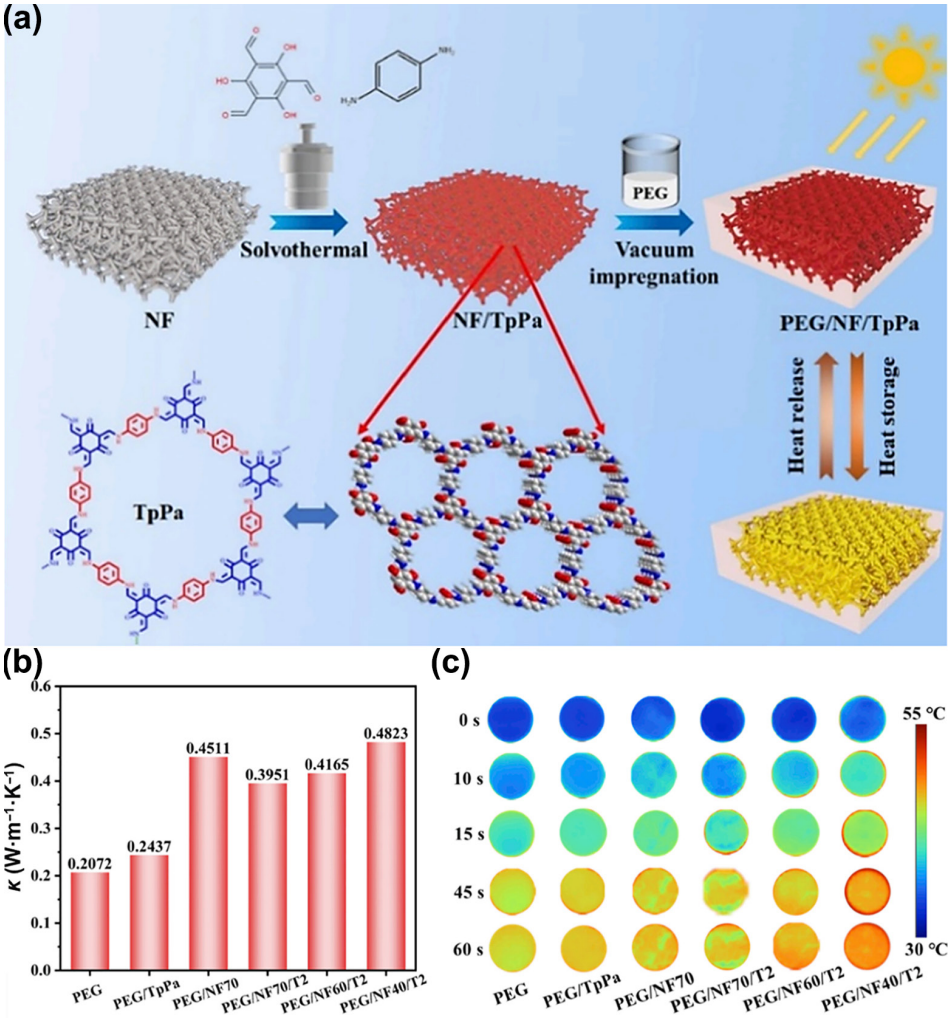

Figure 9 (a) Schematic illustration for the synthesis of PEG/NF/TpPa CPCMs. (b) Thermal conductivity of PEG/NF70, PEG/TpPa, and PEG/NF/TpPa. (c) Infrared thermal image of PEG, PEG/NF70, PEG/TpPa, and PEG/NF/TpPa that are heated on a hot platform of 55 °C. Reproduced with permission from Ref. [77], © Elsevier Ltd. 2023.

3.1 Structural engineering and compositional design

Manipulating the primary framework structure and chemical composition presents profound challenges for thermal management [79, 142, 143]. The intrinsic porosity essential for MOF/COF functionality acts as a primary phonon scattering center, drastically reducing the mean free path of heat carriers. While strong covalent bonds in COFs offer a potential route for higher κ compared to MOFs with weaker coordination bonds, achieving this potential is hindered by their inherent anisotropy and the difficulty in optimizing pore size/shape simultaneously for high adsorption and thermal transport. Introducing heavy atoms (e.g., Si, S) to enhance phonon scattering for low-κ applications is feasible but severely restricts structural diversity and synthetic accessibility. Furthermore, achieving low κ in high-density, large-pore structures remains elusive. The impact of advanced structural features, such as interpenetrated networks prevalent in MOFs and emerging in 3D COFs, on thermal conductivity is virtually unexplored despite its known influence on stability and adsorption, representing a significant knowledge gap. Designing frameworks that reconcile the antagonistic requirements of large, accessible pores and continuous pathways for efficient phonon propagation is a central, unresolved challenge.

3.2 Hurdles in experimental characterization

The inherently ultra-low intrinsic thermal conductivity of MOFs/COFs (often < 1 $W \cdot m^{-1} \cdot K^{-1}$, sometimes < 0.1 $W \cdot m^{-1} \cdot K^{-1}$), stemming from porous structures, weak inter-particle interactions, and pronounced phonon scattering, presents a fundamental measurement difficulty. Experimental results are highly sensitive to sample form, with the dominant form of pressed powders or pellets, introducing substantial uncertainties due to inter-particle contact resistance and porosity effects. Because achieving large, defect-free single crystals or thick homogeneous films that are suitable for accurate characterization is often synthetically challenging. Furthermore, the hygroscopic nature of many MOFs/COFs means adsorbed water can significantly alter thermal transport properties, requiring meticulous environmental control and reporting of hydration state during measurement. Potential anisotropy in single crystals adds complexity but is rarely measured due to the difficulty in obtaining suitable specimens. Collectively, these factors, including ultra-low baseline conductivity, sample form dependence, moisture sensitivity, anisotropy challenges, and limited suitable sample availability, complicate obtaining reliable thermal conductivity data for MOFs/COFs.

3.3 Computational modeling and predictive design

The development of accurate, predictive models for the thermal conductivity of MOFs and COFs, especially when loaded with adsorbates or integrated into composites, faces severe computational hurdles. Traditional theoretical approaches, such as effective medium approximations [29, 144] and mixing rules, fail catastrophically for these systems, significantly overestimating κ by neglecting the complex phonon scattering induced by confined adsorbates and heterogeneous interfaces. Molecular dynamics (MD) simulations are hampered by the lack of accurate [60], transferable force fields capable of describing the diverse interactions within frameworks (particularly metal nodes in MOFs), at organic-inorganic interfaces, and between frameworks and confined guests. The conventional Green-Kubo method [26, 51] suffers from convergence issues with the non-decaying oscillatory thermal conductivity curves typical of these complex systems. Density functional theory (DFT) [145, 146], essential for fundamental electronic and vibrational insights, becomes computationally intractable for the large unit cells (> 1000 atoms) characteristic of MOFs/COFs and their composites. High-throughput simulations [80, 147, 148] have identified some structural features correlating with higher κ (e.g., tetrahedral nodes, vertically oriented ligands), but the underlying physical mechanisms remain opaque. This computational gap severely limits the rational design of materials with tailored thermal properties, forcing reliance on empirical trial-and-error approaches.

4 Pathways for overcoming challenges

The multifaceted challenges in controlling the κ of MOFs and COFs necessitate integrated solutions spanning computational innovation, experimental advancement, and hierarchical structural design. This involves developing highly accurate machine learning [149, 150] potentials trained on high-fidelity quantum mechanical data, creating adaptive algorithms capable of handling convergence in large-scale molecular dynamics (MD) simulations, and establishing robust multiscale modeling frameworks. Simultaneously, the critical hurdle of reliable property measurement demands revolutionizing experimental characterization. Key aspects include pioneering techniques to synthesize and characterize large, high-quality single crystals of COFs [151] and complex MOFs [152]. This is a prerequisite for intrinsic κ measurement, which is based on developing novel *in-situ* probes capable of mapping phonon transport dynamics and guest molecule effects under realistic operational conditions, and creating standardized protocols for measuring intrinsic κ in challenging forms. Finally, unlocking tailored thermal properties necessitates innovating hierarchical design strategies [2] that integrate insights from computation and experiment. Success in these interconnected areas is paramount for harnessing the thermal properties of MOFs and COFs in applications ranging from gas storage and thermal management to energy conversion.

4.1 Advancing computational modeling and high-throughput screening

The vast chemical and structural tunability of MOFs/COFs creates an immense design space, making systematic exploration of structure-thermal property relationships via traditional methods infeasible. Computational challenges are profound: conventional DFT is prohibitively expensive for large unit cells containing hundreds to thousands of atoms, essential for accurate phonon calculations. Alternative methods face significant limitations. Semi-empirical quantum mechanics [55, 153] (e.g., DFTB) suffers from inadequate parameterization, especially for metals. Extended tight-binding methods (e.g., GFN1-*x*TB) scale poorly and lack validation for MOF phonons [52]. Furthermore, as highlighted in recent critiques [154–156], this persistent issue of imaginary frequency phonon modes, which undermines the stability and reliability of predictions, can be effectively optimized or resolved through Active Learning approaches. By iteratively refining training data based on uncertainty sampling, active learning mitigates such artifacts, enhancing model robustness for complex systems like MOFs/COFs. Conventional force fields (e.g., UFF [157], CHARMM [158]) are efficient but lack accuracy for dynamical properties, like phonons across diverse chemistries. Machine learning (ML) [159, 160] potentials show promising performance, while current limitations include specificity to training datasets, the impractical need for continuous DFT retraining for new configurations, and fundamental issues like generating imaginary phonon modes even with advanced models (e.g., MACE-MP-0 [52]). What's more, theoretical models need improvements to better capture anharmonicity (beyond the quasiharmonic approximation), high-frequency vibrations (90–100 THz), and complexities arising from magnetic elements with varying spin states. Consequently, it hinges on developing robust high-throughput computational screening driven by advanced ML potentials trained on high-fidelity fragment-based DFT data. Leveraging existing literature to build comprehensive, robust databases will be a significant catalyst for this effort, enabling accelerated data curation and validation to fuel future ML-driven discoveries. This requires creating adaptive algorithms for efficient MD convergence and accurate κ prediction (improving upon Green-Kubo), establishing rigorous multiscale frameworks linking quantum to mesoscale phenomena, and overcoming current theoretical/modeling inadequacies to enable the rapid, reliable prediction of κ across vast chemical spaces.

This computational power is essential to identify design rules, such as the stringent criteria for high-κ COFs (C–C linkages, density > 500 kg·m^{-3}, porosity 0.6–0.9, pore size < 15 Å, specific surface area, high chain alignment), and explore the broad κ tunability required for diverse applications (from ultralow κ for barriers to high κ for gas storage).

4.2 Revolutionizing experimental characterization techniques

A fundamental barrier to understanding and regulating intrinsic κ is the severe limitation in experimental measurement capabilities, particularly for the often sub-millimeter single crystals typical of MOFs/COFs. Traditional contact-based methods (T-type, 3ω [161], transient thermoreflectance [162, 163]) require large sample dimensions and introduce significant systematic errors due to thermal contact resistance between the sample and sensors. Measurements on compressed powders or pellets yield "effective" κ values dominated by intergranular thermal contact resistance, masking the intrinsic crystal κ. Techniques like flash methods [164] or transient hot-wire methods [165] also typically need millimeter-sized samples, conflicting with MOF/COF synthesis realities. Isolating intrinsic κ from interparticle and grain boundary resistance contributions in powders or composites remains a pervasive challenge. While non-contact methods (e.g., dual-wavelength laser flash Raman spectroscopy [56]) exist for 1D/2D materials, they struggle with micrometer-scale granular samples due

to difficulties in determining heat flux and temperature on heterogeneous surfaces. Solutions, therefore, must focus on pioneering novel *in-situ* characterization techniques. Innovations like the Raman-resistance temperature detector (Raman-RTD) method [50] offer promise by eliminating thermal contact resistance errors. However, overcoming the limitations of such nascent techniques is crucial. This involves extending applicability beyond materials with strong Raman temperature dependence, developing methods for smaller (< 7 μm) and non-spherical crystals requiring complex heat conduction model reconstruction, and creating probes capable of mapping phonon transport and guest molecule effects under operational conditions (high T, P, gas load). Furthermore, establishing standardized protocols for measuring intrinsic κ across different material forms (single crystals, thin films, powders) is essential to generate reliable, comparable data and minimize interfacial artifacts.

4.3 Implementing hierarchical structural design strategies

Translating computational insights and experimental data into materials with tailored κ requires deliberate engineering across multiple structural scales. Key challenges include minimizing thermal boundary (Kapitza) resistance at interfaces, strategically utilizing structural complexity for phonon scattering control, and rationally integrating MOFs/COFs into composite architectures.

Solutions involve sophisticated hierarchical design approaches. At the atomic/molecular scale, this means engineering linker chemistry, bonding, and coordination to influence intrinsic phonon spectra and group velocities. Deliberately designing defects offers a powerful lever to tune phonon scattering, but protocols must be developed to optimize scattering length scales without degrading structural integrity or functionality. Systematically exploring the thermal impact of structural motifs like interpenetration is vital. At the mesoscale, controlling crystal morphology, grain size, and especially grain boundaries is critical for managing phonon scattering and interfacial resistance. For composites [166, 167], the challenge is maximizing synergistic effects. This involves rationally combining materials, for instance, embedding low-κ functional MOF/COF particles or coatings within high-κ continuous matrices (or vice-versa), guided by computational models to optimize interfacial thermal conductance and the overall thermal pathway. Designing interfaces at multiple levels (atomic bonding within the framework, framework-guest interactions, particle-matrix boundaries in composites) to minimize Kapitza resistance is a central tenet. Success requires tight integration of insights gained from advanced computational prediction (guiding linker selection, defect types, composite formulation) and precise experimental validation under relevant conditions.

Effectively regulating the thermal conductivity of MOFs and COFs to meet the divergent demands of applications like gas storage (high κ for heat dissipation), thermal barrier coatings (ultralow κ), or thermoelectrics (optimized κ) is a complex, multifaceted challenge. The solutions lie not in isolated advances, but in a concerted, interdisciplinary approach targeting three critical pillars. Firstly, transformative computational tools for reliable prediction and high-throughput screening across vast chemical spaces. Secondly, revolutionary experimental techniques for accurate, artifact-free κ measurement, especially in challenging forms like single crystals and under operational conditions. Finally, innovative hierarchical design strategies that deliberately engineer structure from the atomic to the macroscopic scale to control phonon transport and interfacial thermal resistance. Progress hinges on the synergistic development of these areas. Advanced computation guides targeted synthesis and design; sophisticated characterization provides ground truth data to validate and refine models; and hierarchical design principles translate fundamental understanding into functional materials. Overcoming the current limitations in each domain is essential to unlock the full potential of these versatile materials for advanced thermal management, energy conversion, and storage technologies.

5 Conclusions

This comprehensive review systematically explores the multifaceted strategies, inherent challenges, and emerging solutions for regulating κ in MOFs and COFs, emphasizing their critical role in thermal management applications such as gas storage, catalysis, electronics, and thermoelectrics. It details key approaches for κ modulation, including: framework architecture engineering to optimize phonon pathways through pore/geometry control, density adjustment, and topology design; pore environment engineering leveraging guest molecule infiltration to dynamically alter thermal transport via competing phonon scattering and guest-phase conduction mechanisms; interfacial bonding enhancement, particularly within COF layers or at MOF composite interfaces, to strengthen vibrational coupling and reduce Kapitza resistance; and composite integration with high-κ additions to create percolating thermal highways. Despite these advances, significant challenges persist, such as the fundamental trade-off between essential porosity (inducing phonon scattering) and efficient phonon propagation, limitations in experimental characterization and computational modeling accuracy, interfacial thermal resistance, and the detrimental impact of defects on κ. Potential solution pathways involve synergistic material design, multidisciplinary integration of advanced synthesis, characterization, and predictive simulations, and leveraging stimuli-responsive frameworks for adaptive thermal control. The review provides a foundational toolkit for rationally tailoring κ over orders of magnitude, enabling MOFs and COFs to overcome thermal limitations and unlock their full potential in next-generation energy and electronic technologies.

Acknowledgements

B. X. acknowledges financial support from the Natural Science Research Start-up Foundation of Recruiting Talents of Nanjing University of Posts and Telecommunications (No. NY225008), the National Natural Science Foundation of China (No. 22375093), Key Laboratory of Advanced Energy Materials Chemistry (Ministry of Education), Nankai University, Key Laboratory of Intelligent Sensing Materials and Chip Integration Technology of Zhejiang Province (No. 2021E10022), Hangzhou Innovation Institute of Beihang University, and State Key Laboratory of Physical Chemistry of Solid Surfaces, Xiamen University. P. F. X. acknowledges financial support from the Natural Science Research Start-up Foundation of Recruiting Talents of Nanjing University of Posts and Telecommunications (No. NY225080).

Declaration of competing interest

All the contributing authors report no conflict of interests in this work.

Author contribution statement

P. F. X.: Data curation, validation, writing – original draft. Y. B.: Validation, software. C. L. L.: Investigation. S. N.: Software. B. X.: Funding acquisition, supervision, writing – review & editing. All the authors have approved the final manuscript.

Use of AI statement

None.

References

[1] Carsch, K. M.; Jiang, H. Z. H.; Klein, R. A.; Rosen, A. S.; Summerhill, P. S.; Peltier, J. L.; Huang, A. J.; Murphy, R. A.; Dods, M. N.; Silva, H. A. et al. Multigas adsorption with single-site cooperativity in a metal-organic framework. *Science* **2025**, *390*, 808–812.

[2] Cao, X. L.; Ji, Y. J.; Li, W. Q.; Gao, H. Y.; Wang, X. Q.; Wang, G. Recent advances in MOF membranes for oil-water separation: From surface and pore engineering to multifunctional applications. *Coord. Chem. Rev.* **2026**, *549*, 217381.

[3] Li, J.; Jing, X. C.; Li, Q. Q.; Li, S. W.; Gao, X.; Feng, X.; Wang, B. Bulk COFs and COF nanosheets for electrochemical energy storage and conversion. *Chem. Soc. Rev.* **2020**, *49*, 3565–3604.

[4] Liu, R. Y.; Zhao, D.; Ji, S. L.; Shao, H. P.; Chen, Y. Z.; Feng, M. J.; Wang, T.; Li, J.; Lin, M.; Sum, T. C. et al. Harvesting singlet and triplet excitation energies in covalent organic frameworks for highly efficient photocatalysis. *Nat. Mater.* **2025**, *24*, 1245–1257.

[5] Jiang, D. L.; Tan, V. G. W.; Gong, Y. F.; Shao, H. P.; Mu, X. Y.; Luo, Z. L.; He, S. Y. Semiconducting covalent organic frameworks. *Chem. Rev.* **2025**, *125*, 6203–6308.

[6] Li, W. Y.; Wang, L. Y.; Keshta, B. E.; Bi, Y. F.; Zhang, Y. B.; Chen, B. L. Recent advances on porous coordination cages for gas storage and separation. *Coord. Chem. Rev.* **2025**, *545*, 217032.

[7] Yu, B. Q.; Tao, Y.; Yao, X.; Jin, Y. C.; Liu, S.; Xu, T. T.; Wang, H. L.; Wu, H.; Zhou, W.; Zhou, X. et al. Single-crystalline 3D covalent organic frameworks with exceptionally high specific surface areas and gas storage capacities. *J. Am. Chem. Soc.* **2024**, *146*, 28932–28940.

[8] Wang, M. D.; Wu, Z. H.; Zhou, G. Z.; Wu, X. Q.; Li, S.; Ma, T. Y.; Ren, Y. X.; Hai, G. T.; Wang, B.; Li, D. S. Partitioning COF membrane channels into ultramicroporous and π-electron-rich compartments for multicomponent ion separations. *Angew. Chem., Int. Ed.* **2025**, *64*, e202514179.

[9] Zhang, Y. M.; Yin, B. H.; Huang, L. Z.; Ding, L.; Lei, S.; G. Telfer, S. ; Caro, J.; Wang, H. H. MOF membranes for gas separations. *Prog. Mater. Sci.* **2025**, *151*, 101432.

[10] Ahmed, I.; Mondol, M. M. H.; Jung, M. J.; Lee, G. H.; Jhung, S. H. MOFs with bridging or terminal hydroxo ligands: Applications in adsorption, catalysis, and functionalization. *Coord. Chem. Rev.* **2023**, *475*, 214912.

[11] Shah, S. S. A.; Javed, M. S.; Najam, T.; Nazir, M. A.; ur Rehman, A.; Rauf, A.; Sohail, M.; Verpoort, F.; Bao, S. J. Covalent Organic Frameworks (COFs) for heterogeneous catalysis: Recent trends in design and synthesis with structure–activity relationship. *Mater. Today* **2023**, *67*, 229–255.

[12] Pham, H. T. B.; Choi, J. Y.; Huang, S. F.; Wang, X. B.; Claman, A.; Stodolka, M.; Yazdi, S.; Sharma, S.; Zhang, W.; Park, J. Imparting functionality and enhanced surface area to a 2D electrically conductive MOF via macrocyclic linker. *J. Am. Chem. Soc.* **2022**, *144*, 10615–10621.

[13] Hu, L. G.; Wu, W. H.; Hu, M.; Jiang, L.; Lin, D. H.; Wu, J.; Yang, K. Double-walled Al-based MOF with large microporous specific surface area for trace benzene adsorption. *Nat. Commun.* **2024**, *15*, 3204.

[14] Zhang, H. Y.; Zhou, Z. H.; Zhu, C. H.; Yaghi, O. M. Crystalline coumarin-linked covalent organic frameworks. *Nat. Synth.* **2025**, *4*, 1376–1385.

[15] Kwon, J.; Ma, H.; Giri, A.; Hopkins, P. E.; Shustova, N. B.; Tian, Z. T. Thermal conductivity of covalent-organic frameworks. *ACS Nano* **2023**, *17*, 15222–15230.

[16] Moayed Mohseni, M.; Jouyandeh, M.; Mohammad Sajadi, S.; Hejna, A.; Habibzadeh, S.; Mohaddespour, A.; Rabiee, N.; Daneshgar, H.; Akhavan, O.; Asadnia, M. et al. Metal-organic frameworks (MOF) based heat transfer: A comprehensive review. *Chem. Eng. J.* **2022**, *449*, 137700.

[17] Rahman, M. A.; Dionne, C. J.; Giri, A. Pore size dictates anisotropic thermal conductivity of two-dimensional covalent organic frameworks with adsorbed gases. *ACS Appl. Mater. Interfaces* **2022**, *14*, 21687–21695.

[18] Babaei, H.; McGaughey, A. J. H.; Wilmer, C. E. Effect of pore size and shape on the thermal conductivity of metal-organic frameworks. *Chem. Sci.* **2017**, *8*, 583–589.

[19] Pelkowski, C. E.; Natraj, A.; Malliakas, C. D.; Burke, D. W.; Bardot, M. I.; Wang, Z. X.; Li, H. Y.; Dichtel, W. R. Tuning crystallinity and stacking of two-dimensional covalent organic frameworks through side-chain interactions. *J. Am. Chem. Soc.* **2023**, *145*, 21798–21806.

[20] Dong, X.; Hou, J. L.; Wang, Z. C.; Ji, J. Q.; Yao, Z. G.; Wang, Y.; Sun, H. C.; Lv, K. X.; Wang, L.; Song, X. et al. Highly sulfonated COF in hybrid PEMs confer efficient proton conductivity for water electrolysis. *J. Membr. Sci.* **2026**, *738*, 124875.

[21] Yang, M. M.; Yasin, S.; Chen, Q.; Peng, W. Z.; Lv, Z. W.; Qi, Z. P.; Shi, J. F. Suppressing high pressure hydrogen blistering in NBR via Zn-based MOF vulcanization: Microstructural and mechanical insights. *Int. J. Hydrogen Energy* **2025**, *181*, 151810.

[22] Wieser, S.; Kamencek, T.; Dürholt, J. P.; Schmid, R.; Bedoya-Martínez, N.; Zojer, E. Identifying the bottleneck for heat transport in metal-organic frameworks. *Adv. Theory Simul.* **2021**, *4*, 2000211.

[23] Ma, H.; Aamer, Z.; Tian, Z. T. Ultrahigh thermal conductivity in three-dimensional covalent organic frameworks. *Mater. Today Phys.* **2021**, *21*, 100536.

[24] Giri, A.; Hopkins, P. E. Heat transfer mechanisms and tunable thermal conductivity anisotropy in two-dimensional covalent organic frameworks with adsorbed gases. *Nano Lett.* **2021**, *21*, 6188–6193.

[25] Islamov, M.; Boone, P.; Babaei, H.; McGaughey, A. J. H.; Wilmer, C. E. Correlated missing linker defects increase thermal conductivity in metal-organic framework UiO-66. *Chem. Sci.* **2023**, *14*, 6592–6600.

[26] Islamov, M.; Babaei, H.; Wilmer, C. E. Influence of missing linker defects on the thermal conductivity of metal-organic framework HKUST-1. *ACS Appl. Mater. Interfaces* **2020**, *12*, 56172–56177.

[27] Thakur, S.; Giri, A. Supramolecular reinforcement drastically enhances thermal conductivity of interpenetrated covalent organic frameworks. *J. Mater. Chem. A* **2023**, *11*, 18660–18667.

[28] He, H. S.; Feng, D. L.; Zhang, X. X.; Feng, Y. H. Transport properties of ZIF-8 nanocrystals for hydrogen adsorption: Molecular dynamics study. *J. Energy Storage* **2023**, *72*, 108270.

[29] Babaei, H.; DeCoster, M. E.; Jeong, M.; Hassan, Z. M.; Islamoglu, T.; Baumgart, H.; McGaughey, A. J. H.; Redel, E.; Farha, O. K.; Hopkins, P. E. et al. Observation of reduced thermal conductivity in a metal-organic framework due to the presence of adsorbates. *Nat. Commun.* **2020**, *11*, 4010.

[30] Zhou, S. Y.; Apostolopoulou-Kalkavoura, V.; Tavares da Costa, M. V.; Bergström, L.; Strømme, M.; Xu, C. Elastic aerogels of cellulose nanofibers@metal-organic frameworks for thermal insulation and fire retardancy. *Nano-Micro Lett.* **2020**, *12*, 9.

[31] Li, Z. R.; Chen, Z. L.; Huang, Q. L.; Zhang, S.; Wang, W.; Li, W. MOF@lignocellulosic nanofibril aerogel designed by carboxymethylated nanocellulose bridging for thermal insulation and fire retardancy. *Adv. Compos. Hybrid Mater.* **2024**, *7*, 28.

[32] Ebrahim, A.; Ghali, M.; El-Moneim, A. A. Microporous Zr-metal-

organic frameworks based-nanocomposites for thermoelectric applications. *Sci. Rep.* **2024**, *14*, 13067.
[33] Fan, Y.; Liu, Z. X.; Chen, G. M. Recent progress in designing thermoelectric metal-organic frameworks. *Small* **2021**, *17*, 2100505.
[34] Feng, D. L.; Feng, Y. H.; Liu, Y. Z.; Zhang, W. S.; Yan, Y. Y.; Zhang, X. X. Thermal conductivity of a 2D covalent organic framework and its enhancement using fullerene 3D self-assembly: A molecular dynamics simulation. *J. Phys. Chem. C* **2020**, *124*, 8386–8393.
[35] Geng, L.; Wang, J. P.; Yang, X. L.; Jiang, J. P.; Li, R.; Yan, Y. B.; Zhao, J. T.; Liu, C. H. Synergistic enhancement of phase change materials through three-dimensional porous layered covalent triazine framework/expanded graphite composites for solar energy storage and beyond. *Chem. Eng. J.* **2024**, *487*, 150749.
[36] Ma, H.; Li, C.; Tian, Z. T. Hydrogen bonds significantly enhance out-of-plane thermal and electrical transport in 2D graphamid: Implications for energy conversion and storage. *ACS Appl. Nano Mater.* **2020**, *3*, 11090–11097.
[37] Zeng, X. L.; Zhou, Y.; Xia, X. N.; Fan, J. F.; Rao, S. P.; Ren, L. L.; Shen, X.; Sun, R.; Zeng, X. L. Elastomer composites with high damping and low thermal resistance via hierarchical interactions and regulating filler. *Small* **2024**, *20*, 2306946.
[38] Naderi, L.; Shahrokhian, S. Ni, S Co-doped Cu dendrites decorated with core-shell architecture assisted by MOF and $Fe_{0.92}Co_{0.08}S$ nanoflakes on nanocellulose/graphene fibers for fabrication of flexible wire-type micro-supercapacitor. *Nanoscale* **2024**, *16*, 20260–20279.
[39] Wiraja, C.; Zhao, Y. L. Toward miniaturizing microelectronics using covalent organic framework dielectric. *Matter* **2021**, *4*, 1760–1762.
[40] Diao, K. L.; Zhou, T.; Zhang, D. H.; Liu, D. J.; Du, J. J.; Zou, K. X.; Qin, S. H. Unlock multi-function: Cnts@COF hydrogel with high toughness, arbitrary shape adaptability, strong electromagnetic shielding and heat insulation performance. *Prog. Org. Coat.* **2025**, *208*, 109469.
[41] Zhang, W. J.; Al-Maythalony, B. A.; Gao, F. X.; Wu, F. S.; Zhao, W.; Xu, P. F.; Zhang, W. H.; Chen, C. L.; Shi, Z.; Wang, X. Y. et al. Thermally stable inorganic $Bi_{0.4}Sb_{1.6}Te_3$/metal-organic framework (MOF) composites with 1-by-1 nm pore engineering towards mid-temperature thermoelectrics. *Energy Environ. Sci.* **2024**, *17*, 5679–5690.
[42] Huang, B. L.; Ni, Z.; Millward, A.; McGaughey, A. J. H.; Uher, C.; Kaviany, M.; Yaghi, O. Thermal conductivity of a metal-organic framework (MOF-5): Part II. *Measurement. Int. J. Heat Mass Transfer* **2007**, *50*, 405–411.
[43] Huang, B. L.; McGaughey, A. J. H.; Kaviany, M. Thermal conductivity of metal-organic framework 5 (MOF-5): Part I. Molecular dynamics simulations. *Int. J. Heat Mass Transfer* **2007**, *50*, 393–404.
[44] Evans, A. M.; Giri, A.; Sangwan, V. K.; Xun, S. N.; Bartnof, M.; Torres-Castanedo, C. G.; Balch, H. B.; Rahn, M. S.; Bradshaw, N. P.; Vitaku, E. et al. Thermally conductive ultra-low-*k* dielectric layers based on two-dimensional covalent organic frameworks. *Nat. Mater.* **2021**, *20*, 1142–1148.
[45] DeCoster, M. E.; Babaei, H.; Jung, S. S.; Hassan, Z. M.; Gaskins, J. T.; Giri, A.; Tiernan, E. M.; Tomko, J. A.; Baumgart, H.; Norris, P. M. et al. Hybridization from guest-host interactions reduces the thermal conductivity of metal-organic frameworks. *J. Am. Chem. Soc.* **2022**, *144*, 3603–3613.
[46] Wieser, S.; Kamencek, T.; Schmid, R.; Bedoya-Martínez, N.; Zojer, E. Exploring the impact of the linker length on heat transport in metal-organic frameworks. *Nanomaterials* **2022**, *12*, 2142.
[47] Ma, T. Q.; Li, J.; Niu, J.; Zhang, L.; Etman, A. S.; Lin, C.; Shi, D. E.; Chen, P. H.; Li, L. H.; Du, X. et al. Observation of interpenetration isomerism in covalent organic frameworks. *J. Am. Chem. Soc.* **2018**, *140*, 6763–6766.
[48] Han, L. P.; Budge, M.; Alex Greaney, P. Relationship between thermal conductivity and framework architecture in MOF-5. *Comput. Mater. Sci.* **2014**, *94*, 292–297.
[49] Babaei, H.; Wilmer, C. E. Mechanisms of heat transfer in porous crystals containing adsorbed gases: Applications to metal-organic frameworks. *Phys. Rev. Lett.* **2016**, *116*, 025902.
[50] Huang, J.; Fan, A. R.; Xia, X. X.; Li, S.; Zhang, X. *In situ* thermal conductivity measurement of single-crystal zeolitic imidazolate framework-8 by Raman-resistance temperature detectors method. *ACS Nano* **2020**, *14*, 14100–14107.
[51] Liu, Y. Z.; Feng, Y. H.; Huang, Z.; Zhang, X. X. Thermal conductivity of 3D boron-based covalent organic frameworks from molecular dynamics simulations. *J. Phys. Chem. C* **2016**, *120*, 17060–17068.
[52] Elena, A. M.; Kamath, P. D.; Jaffrelot Inizan, T.; Rosen, A. S.; Zanca, F.; Persson, K. A. Machine learned potential for high-throughput phonon calculations of metal-organic frameworks. *npj Comput. Mater.* **2025**, *11*, 125.
[53] Thakur, S.; Giri, A. Guiding the design of multifunctional covalent organic frameworks: High-throughput screening of thermal and mechanical properties. *Chem. Mater.* **2025**, *37*, 8978–8995.
[54] Thakur, S.; Giri, A. Pushing the limits of heat conduction in covalent organic frameworks through high-throughput screening of their thermal conductivity. *Small* **2024**, *20*, 2401702.
[55] Siebenmorgen, T.; Menezes, F.; Benassou, S.; Merdivan, E.; Didi, K.; Mourão, A. S. D.; Kitel, R.; Liò, P.; Kesselheim, S.; Piraud, M. et al. MISATO: Machine learning dataset of protein-ligand complexes for structure-based drug discovery. *Nat. Comput. Sci.* **2024**, *4*, 367–378.
[56] Fan, A. R.; Hu, Y. D.; Ma, W. G.; Wang, H. D.; Zhang, X. Dual-wavelength laser flash Raman spectroscopy method for *in-situ* measurements of the thermal diffusivity: Principle and experimental verification. *J. Therm. Sci.* **2019**, *28*, 159–168.
[57] Ying, P. H.; Liang, T.; Xu, K.; Zhang, J.; Xu, J. B.; Zhong, Z.; Fan, Z. Y. Sub-micrometer phonon mean free paths in metal-organic frameworks revealed by machine learning molecular dynamics simulations. *ACS Appl. Mater. Interfaces* **2023**, *15*, 36412–36422.
[58] Sun, L.; Liao, B. L.; Sheberla, D.; Kraemer, D.; Zhou, J. W.; Stach, E. A.; Zakharov, D.; Stavila, V.; Talin, A. A.; Ge, Y. C. et al. A Microporous and naturally nanostructured thermoelectric metal-organic framework with ultralow thermal conductivity. *Joule* **2017**, *1*, 168–177.
[59] Wieme, J.; Vandenbrande, S.; Lamaire, A.; Kapil, V.; Vanduyfhuys, L.; Van Speybroeck, V. Thermal engineering of metal-organic frameworks for adsorption applications: A molecular simulation perspective. *ACS Appl. Mater. Interfaces* **2019**, *11*, 38697–38707.
[60] Shi, W.; Liu, C. X.; Wen, Y. M.; Dong, F. X.; Wu, X. M.; Deng, T. Q.; Yu, H. D.; Yang, J.; Xi, J. Y. Probing the origin of 2D covalent organic frameworks with high thermoelectric performance down to the ångström level. *Adv. Funct. Mater.* **2026**, *36*, e15828.
[61] Wang, T.; Zhang, Y. S.; Wang, S.; Wang, T. H.; Geng, S. B.; Chen, Y.; Cheng, P.; Zhang, Z. J. A class of crystalline porous thermosetting polymers: Scalable thermomolding synthesis and propylene purification. *Sci. China Chem.* **2025**, *68*, 2582–2588.
[62] Zhang, X. L.; Jiang, J. W. Thermal conductivity of zeolitic imidazolate framework-8: A molecular simulation study. *J. Phys. Chem. C* **2013**, *117*, 18441–18447.
[63] Laurenz, E.; Füldner, G.; Velte, A.; Schnabel, L.; Schmitz, G. Frequency response analysis for the determination of thermal conductivity and water transport in MOF adsorbent coatings for heat transformation. *Int. J. Heat Mass Transfer* **2021**, *169*, 120921.
[64] Guo, J. Q.; Zhang, D.; Liu, L. L.; Li, Q.; Fang, Y. J.; Bai, P. J.; Bo, Y. W.; Zhou, Y. T.; Wang, G. F.; Ma, R. J. Highly ductile N-type thermoelectric MOF-based foams. *ACS Nano* **2025**, *19*, 29448–29461.
[65] Huang, J.; Xia, X. X.; Hu, X. J.; Li, S.; Liu, K. A general method for

measuring the thermal conductivity of MOF crystals. *Int. J. Heat Mass Transfer* **2019**, *138*, 11–16.

[66] Purewal, J.; Liu, D.; Sudik, A.; Veenstra, M.; Yang, J.; Maurer, S.; Müller, U.; Siegel, D. J. Improved hydrogen storage and thermal conductivity in high-density MOF-5 composites. *J. Phys. Chem. C* **2012**, *116*, 20199–20212.

[67] Qi, X.; Wang, Y. Z.; Li, K. C.; Wang, J.; Zhang, H. L.; Yu, C.; Wang, H. Enhanced electrical properties and restrained thermal transport in p- and n-type thermoelectric metal-organic framework hybrids. *J. Mater. Chem. A* **2021**, *9*, 310–319.

[68] Olorunyomi, J. F.; Dyett, B. P.; Murdoch, B. J.; Ahmed, A. J.; Rosengarten, G.; Caruso, R. A.; Doherty, C. M.; Mulet, X. Simultaneous enhancement of electrical conductivity and porosity of a metal-organic framework toward thermoelectric applications. *Adv. Funct. Mater.* **2024**, *34*, 2403644.

[69] Lin, M. H.; Hsu, C. H.; Kang, D. Y.; Liu, C. L. Correlating framework structures and thermoelectric performance of metal-organic framework/carbon nanotube thermoelectric hybrids with n–p type inversion. *Chem. Eng. J.* **2024**, *485*, 149732.

[70] Lin, C. Y.; Chang, J. W.; Lin, M. H.; Wu, K. C.; Hong, S. H.; Lin, J. M.; Kung, C. W.; Liu, C. L. Carbon nanotube/two-dimensional metal-organic framework composites with enhanced thermoelectric performances for thermoelectric generators. *Chem. Eng. J.* **2025**, *521*, 166861.

[71] Cui, B. Y.; Audu, C. O.; Liao, Y. J.; Nguyen, S. T.; Farha, O. K.; Hupp, J. T.; Grayson, M. Thermal conductivity of ZIF-8 thin-film under ambient gas pressure. *ACS Appl. Mater. Interfaces* **2017**, *9*, 28139–28143.

[72] Ying, P. H.; Zhang, J.; Zhang, X.; Zhong, Z. Impacts of functional group substitution and pressure on the thermal conductivity of ZIF-8. *J. Phys. Chem. C* **2020**, *124*, 6274–6283.

[73] Fang, M.; He, R. Q.; Zhou, J. D.; Fei, H.; Yang, K. Thermal conductivity enhancement and shape stability of composite phase change materials using MIL-101(Cr)-NH_2/expanded graphite/multi-walled carbon nanotubes. *J. Energy Storage* **2024**, *86*, 111244.

[74] Chen, D. L.; Sha, J. C.; Mei, X. D.; Ye, A.; Zhao, Z. P.; Qiu, X. L.; Liu, X.; Niu, Y. P.; Zuo, P. Y.; Zhuang, Q. X. Ultralow *k* covalent organic frameworks enabling high fidelity signal transmission and high temperature electromechanical sensing. *Nat. Commun.* **2024**, *15*, 10864.

[75] Li, K.; Ma, H. Decoding the thermal conductivity of ionic covalent organic frameworks: Optical phonons as key determinants revealed by neuroevolution potential. *Mater. Today Phys.* **2025**, *54*, 101724.

[76] Li, X. Q.; Lv, G. X.; Hu, Y. L.; Tsao, Y. H.; Hu, R. J.; Tian, Z. T.; Liu, K. J.; Ma, H. High through-thickness thermal conductivity in an edge-on two-dimensional polyamide thin film. *Nano Lett.* **2025**, *25*, 8948–8953.

[77] Yang, R. Y.; Zheng, N. N.; Yu, Z. X.; Zhang, F. Y.; Gai, H. M.; Chen, J. K.; Huang, X. B. Nickel foam/covalent-organic frameworks for composite phase change materials with enhanced solar-thermal energy conversion and storage capacity. *Appl. Therm. Eng.* **2023**, *230*, 120808.

[78] Giri, A.; Evans, A. M.; Rahman, M. A.; McGaughey, A. J. H.; Hopkins, P. E. Highly negative Poisson's ratio in thermally conductive covalent organic frameworks. *ACS Nano* **2022**, *16*, 2843–2851.

[79] Moscarello, E. M.; Wooten, B. L.; Sajid, H.; Tichenor, L. D.; Heremans, J. P.; Addicoat, M. A.; McGrier, P. L. Thermal conductivity of two-dimensional benzobisoxazole-linked covalent organic frameworks with nanopores: Implications for thermal management applications. *ACS Appl. Nano Mater.* **2022**, *5*, 13787–13793.

[80] Islamov, M.; Babaei, H.; Anderson, R.; Sezginel, K. B.; Long, J. R.; McGaughey, A. J. H.; Gomez-Gualdron, D. A.; Wilmer, C. E. High-throughput screening of hypothetical metal-organic frameworks for thermal conductivity. *npj Comput. Mater.* **2023**, *9*, 11.

[81] Thakolkaran, P.; Zheng, Y.; Guo, Y.; Vashisth, A.; Kumar, S. Deep learning reveals key predictors of thermal conductivity in covalent organic frameworks. *Digital Discovery* **2025**, *4*, 3351–3362.

[82] Rahman, M. A.; Thakur, S.; Hopkins, P. E.; Giri, A. Engineering the electronic and thermal properties of two-dimensional covalent organic frameworks. *J. Phys. Chem. C* **2023**, *127*, 11157–11166.

[83] Lin, Y. C.; Cheng, R. H.; Liang, T. G.; Wu, W. X.; Li, S.; Li, W. Understanding the influence of secondary building units on the thermal conductivity of metal-organic frameworks via high-throughput computational screening. *Phys. Chem. Chem. Phys.* **2023**, *25*, 32407–32415.

[84] Kim, S.; Kim, T. High thermal conductivity dominated by thermal phonons with mean free paths exceeding hundred nanometers in three-dimensional covalent organic framework derivatives: A molecular dynamics study. *J. Phys. Chem. C* **2025**, *129*, 14614–14621.

[85] Wieser, S.; Zojer, E. Machine learned force-fields for an *ab-initio* quality description of metal-organic frameworks. *npj Comput. Mater.* **2024**, *10*, 18.

[86] Zhou, J. D.; Fang, M.; Yang, K.; Lu, K. Q.; Fei, H.; Mu, P.; He, R. Q. MIL-101(Cr)-NH_2/reduced graphene oxide composite carrier enhanced thermal conductivity and stability of shape-stabilized phase change materials for thermal energy management. *J. Energy Storage* **2022**, *52*, 104827.

[87] Li, H. F.; Li, H.; Xun, S. N.; Brédas, J. L. Doping modulation of the charge injection barrier between a covalent organic framework monolayer and graphene. *Chem. Mater.* **2020**, *32*, 9228–9237.

[88] Keypour, H.; Kouhdareh, J.; Alavinia, S.; Karimi-Nami, R.; Karakaya, I.; Rabiei, K. Development of sustainable green catalysts for oxidation of alcohols via decorated palladium nanoparticles on magnetic carbon nanotube/MOF. *J. Mol. Struct.* **2023**, *1294*, 136444.

[89] Xie, L. S.; Skorupskii, G.; Dincă, M. Electrically conductive metal-organic frameworks. *Chem. Rev.* **2020**, *120*, 8536–8580.

[90] Zhao, C. F.; Diercks, C. S.; Zhu, C. H.; Hanikel, N.; Pei, X. K.; Yaghi, O. M. Urea-linked covalent organic frameworks. *J. Am. Chem. Soc.* **2018**, *140*, 16438–16441.

[91] Andreo, J.; Priola, E.; Alberto, G.; Benzi, P.; Marabello, D.; Proserpio, D. M.; Lamberti, C.; Diana, E. Autoluminescent metal-organic frameworks (MOFs): Self-photoemission of a highly stable thorium MOF. *J. Am. Chem. Soc.* **2018**, *140*, 14144–14149.

[92] Li, Z. P.; Wang, Z. Y.; Zhao, S. L.; Seo, J. M.; Li, C. Q.; Jin, Y. C.; Lyu, S. L.; Li, J.; Tang, F.; Kim, W. Y. et al. Alkoxy side chain engineering in metal-free covalent organic frameworks for efficient oxygen reduction. *Adv. Mater.* **2025**, *37*, 2501603.

[93] Tan, F. L.; Han, S.; Peng, D. L.; Wang, H. L.; Yang, J.; Zhao, P.; Ye, X. J.; Dong, X.; Zheng, Y. Y.; Zheng, N. et al. Nanoporous and highly thermal conductive thin film of single-crystal covalent organic frameworks ribbons. *J. Am. Chem. Soc.* **2021**, *143*, 3927–3933.

[94] Vo, P.; Haranczyk, M. Insights into thermal conductivity at the MOF-polymer interface. *ACS Appl. Mater. Interfaces* **2024**, *16*, 56221–56231.

[95] Huang, R.; Yan, Y.; Jiang, Y. F.; Gu, C. Y.; Ma, Z. T.; Xue, L. F.; Ma, Y.; Lin, X. E.; Zhang, J.; Shi, R. et al. A copper-based single-atom material effectively controls plant diseases with nearly zero soil residue and low phytotoxicity. *Sci. Bull.* **2025**, *70*, 3190–3201.

[96] Zhang, J.; Wang, Z. H.; Lin, X. G.; Gao, X. P.; Wang, Q. P.; Huang, R.; Ruan, Y. E.; Xu, H. N.; Tian, L.; Ling, C. et al. Mn−Ce symbiosis: Nanozymes with multiple active sites facilitate scavenging of reactive oxygen species (ROS) based on electron transfer and confinement anchoring. *Angew. Chem., Int. Ed.* **2025**, *64*, e202416686.

[97] Chu, X. Y.; Liu, S. K.; Luan, B. B.; Zhang, Y.; Xi, Y. M.; Shao, L. H.; Zhang, F. M.; Lan, Y. Q. Crystal-facet-controlled internal electric field in MOF/COF heterojunction towards efficient photocatalytic overall water splitting. *Angew. Chem., Int. Ed.* **2025**, *64*, e202422940.

[98] Cai, J. Y.; Zhao, H.; Liu, H.; Wei, Y. F.; Zheng, Z. R.; Zhang, C. N.;

Xiao, L. Q.; Zhao, R.; Hou, L. X. Magnetic field vertically aligned Co-MOF-74 derivatives/polyacrylamide hydrogels with bifunction of excellent electromagnetic wave absorption and efficient thermal conduction performances. *Compos. Part A: Appl. Sci. Manuf.* **2024**, *176*, 107832.

[99] Yang, D. R.; Zuo, S. W.; Yang, H. Z.; Zhou, Y.; Lu, Q. C.; Wang, X. Tailoring layer number of 2D porphyrin-based MOFs towards photocoupled electroreduction of CO_2. *Adv. Mater.* **2022**, *34*, 2107293.

[100] Kim, T. W.; Jun, S.; Ha, Y.; Yadav, R. K.; Kumar, A.; Yoo, C. Y.; Oh, I.; Lim, H. K.; Shin, J. W.; Ryoo, R. et al. Ultrafast charge transfer coupled with lattice phonons in two-dimensional covalent organic frameworks. *Nat. Commun.* **2019**, *10*, 1873.

[101] Zhang, D. B.; Li, J. G.; Ren, Y. H.; Sun, T. Green-Kubo formalism for thermal conductivity with Slater-Koster tight binding. *Phys. Rev. B* **2023**, *108*, 104307.

[102] Kang, J.; Wang, L. W. First-principles Green-Kubo method for thermal conductivity calculations. *Phys. Rev. B* **2017**, *96*, 020302.

[103] Leith, G. A.; Martin, C. R.; Mayers, J. M.; Kittikhunnatham, P.; Larsen, R. W.; Shustova, N. B. Confinement-guided photophysics in MOFs, COFs, and cages. *Chem. Soc. Rev.* **2021**, *50*, 4382–4410.

[104] Hamon, L.; Serre, C.; Devic, T.; Loiseau, T.; Millange, F.; Férey, G.; Weireld, G. D. Comparative study of hydrogen sulfide adsorption in the MIL-53(Al, Cr, Fe), MIL-47(V), MIL-100(Cr), and MIL-101(Cr) metal-organic frameworks at room temperature. *J. Am. Chem. Soc.* **2009**, *131*, 8775–8777.

[105] Sun, R.; Gu, H. Y.; Zhang, Y. Z.; Li, H. G.; Tang, D. H.; Xu, M. Y.; Ma, J. Y.; Song, L. X. Flexible and gradually bonded metal organic framework coatings for atomic oxygen protection of polyimide films. *Appl. Surf. Sci.* **2023**, *641*, 158490.

[106] Zhang, H.; Xiao, F.; Han, H. B.; Wu, Y. H. Fluorinated MIL-53(Al) with breathing effect incorporated mixed matrix membranes for enhanced butanol/water pervaporation performance. *J. Membr. Sci.* **2025**, *713*, 123261.

[107] Thaggard, G. C.; Maldeni Kankanamalage, B. K. P.; Lim, J.; Shi, X. N.; Arnold, V. S.; Badiger, M.; Mulkerrin, R.; Broskey, R. D.; Irizarry, E.; Atim, G. et al. Altering the thermodynamics of stimuli-responsive derivatives through layered hybrid material design. *J. Am. Chem. Soc.* **2025**, *147*, 42591–42606.

[108] Liu, Y. D.; Mostaghimi, M.; Chandresh, A.; Jana, S.; Wenzel, W.; Heinke, L. Photoswitchable conductive metal-organic frameworks. *Adv. Funct. Mater.*, in press, DOI: 10.1002/adfm.202423539.

[109] Sun, Q.; Du, J. C.; Yao, A. Y.; Zhang, Y. T.; Yu, B. Z.; Lim, W.; Hassan, S. U.; Guan, J.; Dou, P. J.; Liu, J. T. Tunable hydrated channels in covalent organic framework membrane for seawater desalination. *ACS Nano* **2025**, *19*, 18409–18420.

[110] Zhao, Y. L.; Tao, X. F.; Lin, J. P.; Lin, S. L. Azobenzene functionalized organic covalent frameworks: Controlled morphologies and photo-regulated adsorption. *Adv. Funct. Mater.* **2023**, *33*, 2302225.

[111] Semelsberger, T. A.; Veenstra, M.; Dixon, C. Room temperature thermal conductivity measurements of neat MOF-5 compacts with high pressure hydrogen and helium. *Int. J. Hydrogen Energy* **2016**, *41*, 4690–4702.

[112] Li, Z. P.; Wang, X. J.; Zhao, S. L.; Li, C. Q.; Kim, W. Y.; Jin, Y. C.; Tang, F.; Jeon, J. P.; Lyu, S. L.; Lee, S. Y. et al. Tuning electrochemical properties of metal-free covalent organic frameworks through hydrogen-bonding interactions. *Adv. Funct. Mater.*, in press, DOI: 10.1002/adfm.202520634.

[113] Wei, D. X.; Zhao, W. Y.; Tian, Z. B.; Zhi, Y. F.; Zhang, Y. W.; Liu, X. M. Fluorescence-enhanced covalent organic frameworks via hydrogen bonding interactions for bisphenol a detection and removal. *ACS Appl. Polym. Mater.* **2024**, *6*, 14688–14694.

[114] Liu, C.; Chen, H. L.; Chen, Q.; Bi, J. H.; Yu, J. C.; Wu, L. Active site modulation in UiO-66(Ce) MOFs by Al^{3+} doping for boosting photocatalysis. *J. Catal.* **2024**, *437*, 115670.

[115] Ghanavati, R.; Escobosa, A. C.; Manz, T. A. An automated protocol to construct flexibility parameters for classical forcefields: Applications to metal-organic frameworks. *RSC Adv.* **2024**, *14*, 22714–22762.

[116] Chen, H. L.; Liu, C.; Guo, W.; Wang, Z. W.; Shi, Y. Z.; Yu, Y.; Wu, L. Functionalized UiO-66(Ce) for photocatalytic organic transformation: The role of active sites modulated by ligand functionalization. *Catal. Sci. Technol.* **2022**, *12*, 1812–1823.

[117] Croy, A.; Raptakis, A.; Bodesheim, D.; Dianat, A.; Cuniberti, G. Toward coarse-grained elasticity of single-layer covalent organic frameworks. *J. Phys. Chem. C* **2022**, *126*, 18943–18951.

[118] Ji, Y. Q.; Lv, H. F.; Wu, X. J. Carrier-induced room-temperature half-metallicity in an exfoliable two-dimensional $Cr(TCNB)_2$ metal-organic framework. *J. Phys. Chem. Lett.* **2025**, *16*, 378–383.

[119] Formalik, F.; Fischer, M.; Kuchta, B. Correlating phonons and deformations: A method for structural phase transformation analysis in metal-organic frameworks. *Cryst. Growth Des.* **2023**, *23*, 8962–8971.

[120] Fu, A.; Yi, G. Z.; Li, Y. Phonon-limited electron transport in a highly conductive two-dimensional covalent organic framework: A computational study. *J. Phys. Chem. C* **2022**, *126*, 20127–20134.

[121] Haeri, Z.; Ramezanzadeh, M.; Ramezanzadeh, B. Ce-TA MOF assembled GO nanosheets reinforced epoxy composite for superior thermo-mechanical properties. *J. Taiwan Inst. Chem. Eng.* **2021**, *126*, 313–323.

[122] Ghohrodi, A. R.; Ramezanzadeh, M.; Ramezanzadeh, B. Investigating the thermo-mechanical and UV-shielding properties of a nano-porous Zr(IV)-type metal-organic framework (MOF) incorporated epoxy composite coating. *Prog. Org. Coat.* **2022**, *164*, 106693.

[123] Wang, S.; Chen, X.; Xia, W. K. Preparation of alkali metal-doped MOF-5@GO composites and study on absorption properties. *ChemistrySelect* **2025**, *10*, e05986.

[124] Zhou, Q.; Hussain, S.; Hu, J. S.; Zhang, G. H.; Zhang, W. X.; Zhang, B.; Wang, L. Polybenzimidazole composite separators engineered from MOFs-HNTs composites applicated in lithium-ion batteries. *Small* **2025**, *21*, 2502051.

[125] Li, S.; Yu, X.; Liu, L. M.; Zhou, L. Q.; Jia, Z. W.; Chen, J. M.; Zhao, Z. X.; Zhao, Z. X. Thermal-conductive MOFs@BN self-supporting foams for synchronously boosting CO_2 adsorption/desorption. *Adv. Funct. Mater.* **2024**, *34*, 2401955.

[126] Qingrong, Z.; Weidong, Z.; Xuan, Z.; Mengbo, W.; Shengping, L. Evaluation of the effects of heat conducting enhancement measures on MOFs hydrogen storage system for ship's propulsion plant. *Int. J. Hydrogen Energy* **2021**, *46*, 18412–18422.

[127] Zhang, H.; Zhao, W. Q.; Wu, Y. Z.; Wang, Y. S.; Zou, M. C.; Cao, A. Y. Dense monolithic MOF and carbon nanotube hybrid with enhanced volumetric and areal capacities for lithium-sulfur battery. *J. Mater. Chem. A* **2019**, *7*, 9195–9201.

[128] Zhu, Q. Q.; Li, H. K.; Sun, X. L.; Han, Z. Y.; Sun, J. C.; He, H. M. Rational incorporation of covalent organic framework/carbon nanotube (COF/CNT) composites for electrochemical aptasensing of ultra-trace atrazine. *J. Mater. Chem. C* **2021**, *9*, 8043–8050.

[129] Weare, B. L.; Lodge, R. W.; Zyk, N.; Weilhard, A.; Housley, C. L.; Strutyński, K.; Melle-Franco, M.; Mateo-Alonso, A.; Khlobystov, A. N. Imaging and analysis of covalent organic framework crystallites on a carbon surface: A nanocrystalline scaly COF/nanotube hybrid. *Nanoscale* **2021**, *13*, 6834–6845.

[130] Dao, X. L.; Nie, M.; Sun, H.; Dong, W.; Xue, Z. H.; Li, Q.; Liao, J. M.; Wang, X. X.; Zhao, X.; Yang, D. X. et al. Electrochemical performance of metal-organic framework MOF(Ni) doped graphene. *Int. J. Hydrogen Energy* **2022**, *47*, 16741–16749.

[131] Rehman, A. U.; Asghar, M.; Rauf, A.; Najam, T.; Shaaban, I. A.; Shah, S. S. A.; Nazir, M. A. MOF/Graphene interfaces in catalytic water splitting: Recent breakthroughs and future outlook. *Fuel* **2026**, *405*, 136800.

[132] Shariat Panahi, S. F. K.; Alihosseini, M.; Neek-Amal, M. Electronic and optical properties of COFs/graphene and COF/hBN

heterostructures. *J. Appl. Phys.* **2024**, *135*, 214302.
[133] Lin, X. G.; Ma, X. Y.; He, Y. S.; Li, S. J.; Chen, W. Z.; Li, L. One-pot construction of metal nanoparticles loaded COF catalysts for aqueous hydrogenation reactions. *Chem.—Eur. J* **2024**, *30*, e202303505.
[134] Gharanli, S.; Malekshah, R. E.; Moharramnejad, M.; Ehsani, A.; Shahi, M.; Joshaghani, A. H.; Amini, A. H.; Haribabu, J.; Istifli, E. S.; Tehrani, F. K. Recent progress in designing heterogeneous COFs with the photocatalytic performance. *Mol. Catal.* **2024**, *560*, 114127.
[135] Kang, Z. X.; Peng, Y. W.; Hu, Z. G.; Qian, Y. H.; Chi, C. L.; Yeo, L. Y.; Tee, L.; Zhao, D. Mixed matrix membranes composed of two-dimensional metal-organic framework nanosheets for pre-combustion CO_2 capture: A relationship study of filler morphology versus membrane performance. *J. Mater. Chem. A* **2015**, *3*, 20801–20810.
[136] Lin, R. J.; Ge, L.; Diao, H.; Rudolph, V.; Zhu, Z. H. Propylene/propane selective mixed matrix membranes with grape-branched MOF/CNT filler. *J. Mater. Chem. A* **2016**, *4*, 6084–6090.
[137] Kang, Z. X.; Wang, S. S.; Wang, R. M.; Guo, H. L.; Xu, B.; Feng, S.; Fan, L. L.; Zhu, L. K.; Kang, W. P.; Pang, J. et al. Sandwich membranes through a two-dimensional confinement strategy for gas separation. *Mater. Chem. Front.* **2018**, *2*, 1911–1919.
[138] Li, Z. Y.; Yu, B. B.; Wang, Y. T.; Yan, B.; Liu, J. Y.; Liu, Y. N.; Wang, R. K.; Rao, P. H.; Liu, Y. Reliable strategy for the covalent bonding of MOFs to SiC membranes for ultrastable noble metal capture in harsh environments. *ACS Appl. Mater. Interfaces* **2025**, *17*, 52981–52992.
[139] Tao, Y. Z.; Wang, L.; Li, B. X.; Huang, J.; Pan, Y. C. Engineering gas-permeable MOF/polymer interfaces in mixed-matrix membranes for advanced CO_2 separation. *J. Membr. Sci.* **2025**, *735*, 124588.
[140] Feng, J. Y.; Wei, Y. Z.; Li, X.; Wang, Q. F.; Wang, B. L.; Guo, Y. Y.; Feng, B. Y.; Jin, E. Q.; Yu, J. H. 3D-Printed COF/zeolite composites for augmented photocatalytic hydrogen peroxide production. *Angew. Chem., Int. Ed.* **2025**, *64*, e202508226.
[141] Ren, X. Y.; Huang, K. H.; Wei, Y. X.; Cai, M.; Li, M. J.; Shen, R. C.; Li, X.; Shao, G. S.; Miao, F. J. 2D/2D COF/MOF S-scheme heterojunction boosts photocatalytic H_2 evolution. *J. Mater. Sci. Technol.* **2026**, *265*, 320–327.
[142] Luo, S.; Tian, X. H.; Pan, L.; Zhou, R. H.; Zhu, S. D.; Yan, Z. Y.; Rao, K.; Liu, B.; Wang, S. F.; Wu, H. Humidity/photothermal dual-responsive TpPa–SO_3H/Ag@MXene actuator for intelligent thermal management. *Mater. Sci. Eng.: R: Rep.* **2026**, *167*, 101125.
[143] Zhang, J.; Liu, Y.; Hu, Y.; Han, W. K.; Fu, J. X.; Zhu, R. M.; Pang, H.; Zhang, J. W.; Gu, Z. G. Covalent organic frameworks with regulated water adsorption sites for efficient cooling of electronics. *ChemSusChem* **2025**, *18*, e202402441.
[144] Novitsky, A.; Ramanovich, M.; Novitsky, D. V. Operator effective medium approximation for inhomogeneous and curvilinear media. *Phys. Rev. B* **2023**, *108*, 205401.
[145] Kashyap, A. Density functional theory and material databases in the era of machine learning. *Appl. Phys. Lett.* **2024**, *125*, 220502.
[146] Chen, G.; Li, Z. Q.; Huang, Z. H.; Lu, H. L.; Long, G. K.; Lezama Pacheco, J. S.; Tok, J. B. H.; Gao, T. Z.; Lei, Y. S.; Zhou, J. Y. et al. Effects of transition metals on metal-octaaminophthalocyanine-based 2D metal-organic frameworks. *ACS Nano* **2023**, *17*, 9611–9621.
[147] Daglar, H.; Keskin, S. Recent advances, opportunities, and challenges in high-throughput computational screening of MOFs for gas separations. *Coord. Chem. Rev.* **2020**, *422*, 213470.
[148] Lan, Y. S.; Han, X. H.; Tong, M. M.; Huang, H. L.; Yang, Q. Y.; Liu, D. H.; Zhao, X.; Zhong, C. L. Materials genomics methods for high-throughput construction of COFs and targeted synthesis. *Nat. Commun.* **2018**, *9*, 5274.
[149] Aksu, G. O.; Keskin, S. The COF space: Materials features, gas adsorption, and separation performances assessed by machine learning. *ACS Mater. Lett.* **2025**, *7*, 954–960.
[150] Gulbalkan, H. C.; Uzun, A.; Keskin, S. Combining computational screening and machine learning to explore MOFs and COFs for methane purification. *Appl. Phys. Lett.* **2024**, *124*, 200501.
[151] Dong, R. H.; Feng, X. L. Making large single crystals of 2D MOFs. *Nat. Mater.* **2021**, *20*, 122–123.
[152] Chen, X. F.; Zhang, X. F.; Leng, C.; Jiang, C.; Gong, W.; Liu, Y.; Cui, Y. Helical polymer metal-organic framework hybrids. *Nat. Synth.* **2026**, *5*, 46–54.
[153] Hunt, P.; Hosseini-Gerami, L.; Chrien, T.; Plante, J.; Ponting, D. J.; Segall, M. Predicting pK_a using a combination of semi-empirical quantum mechanics and radial basis function methods. *J. Chem. Inf. Model.* **2020**, *60*, 2989–2997.
[154] Ouyang, X. J.; Wang, Z. L.; Jie, X.; Zhang, F.; Zhang, Y. X.; Liu, L. J.; Wang, D. W. Latent space active learning with message passing neural network: The case of HfO_2. *Phys. Rev. Mater.* **2024**, *8*, 103804.
[155] Rodriguez, A.; Lin, C. P.; Yang, H.; Al-Fahdi, M.; Shen, C.; Choudhary, K.; Zhao, Y.; Hu, J. J.; Cao, B. Y.; Zhang, H. B. et al. Million-scale data integrated deep neural network for phonon properties of heuslers spanning the periodic table. *npj Comput. Mater.* **2023**, *9*, 20.
[156] Wang, Q.; Zeng, Z. Z.; Chen, Y. Revisiting phonon transport in perovskite $SrTiO_3$: Anharmonic phonon renormalization and four-phonon scattering. *Phys. Rev. B* **2021**, *104*, 235205.
[157] Artemova, S.; Jaillet, L.; Redon, S. Automatic molecular structure perception for the universal force field. *J. Comput. Chem.* **2016**, *37*, 1191–1205.
[158] Beu, T. A.; Ailenei, A. E.; Farcaş, A. CHARMM force field for protonated polyethyleneimine. *J. Comput. Chem.* **2018**, *39*, 2564–2575.
[159] Thiyagalingam, J.; Shankar, M.; Fox, G.; Hey, T. Scientific machine learning benchmarks. *Nat. Rev. Phys.* **2022**, *4*, 413–420.
[160] Xia, J. F.; Zhang, Y. L.; Jiang, B. The evolution of machine learning potentials for molecules, reactions and materials. *Chem. Soc. Rev.* **2025**, *54*, 4790–4821.
[161] Rodrigo, O.; Garnier, B. Thermal contact resistance measurement between two intersecting PAN type carbon fibers using the T-type 3ω method. *Int. J. Therm. Sci.* **2023**, *193*, 108510.
[162] Qu, S. L.; Li, Y. F.; Wang, Z. G.; Jia, Y. Z.; Li, C.; Xu, B.; Chen, W. Q.; Bai, S. Y.; Huang, Z. X.; Tang, Z. N. et al. Thermal conductivity measurement of the He-ion implanted layer of W using transient thermoreflectance technique. *J. Nucl. Mater.* **2017**, *484*, 382–385.
[163] Jeong, J.; Meng, X. H.; Rockwell, A. K.; Bank, S. R.; Hsieh, W. P.; Lin, J. F.; Wang, Y. G. Picosecond transient thermoreflectance for thermal conductivity characterization. *Nanoscale Microscale Thermophys. Eng.* **2019**, *23*, 211–221.
[164] Nomura, T.; Zhu, C. Y.; Nan, S.; Tabuchi, K.; Wang, S. F.; Akiyama, T. High thermal conductivity phase change composite with a metal-stabilized carbon-fiber network. *Appl. Energy* **2016**, *179*, 1–6.
[165] Assael, M. J.; Antoniadis, K. D.; Tzetzis, D. The use of the transient hot-wire technique for measurement of the thermal conductivity of an epoxy-resin reinforced with glass fibres and/or carbon multi-walled nanotubes. *Compos. Sci. Technol.* **2008**, *68*, 3178–3183.
[166] Sun, X.; Wu, S.; Wang, J. J.; Yang, J. C.; Tian, S.; Hu, Q. Z.; Chang, L.; Wang, Z.; Sun, Y. Z.; Wang, Y. B. et al. Hierarchical structural design of cobalt sulphide nanoparticles/nickel sulphide for high-performance supercapacitors. *Chem. Eng. J.* **2024**, *500*, 157393.
[167] Hou, Y.; Wang, J. X.; Chen, B. J.; Zhang, H.; Xiang, Z. C.; Zhu, H. K.; Wang, L. X. Self-standing MOF-derived Co@SiCnw nanocomposite aerogel with a hierarchical microstructure for highly effective and wideband electromagnetic attenuation. *ACS Appl. Mater. Interfaces* **2025**, *17*, 28503–28513.